(12) INTERNATIONAL APPLICATION PUBLISHED UNDER THE PATENT COOPERATION TREATY (PCT)

(19) World Intellectual Property Organization
International Bureau

(43) International Publication Date
3 March 2016 (03.03.2016)

WIPO | PCT

(10) International Publication Number
WO 2016/030750 A1

(51) International Patent Classification:
B01J 13/00 (2006.01)

(21) International Application Number:
PCT/IB2015/001691

(22) International Filing Date:
24 August 2015 (24.08.2015)

(25) Filing Language: English

(26) Publication Language: English

(30) Priority Data:
62/041,323 25 August 2014 (25.08.2014) US

(71) Applicant: **KING ABDULLAH UNIVERSITY OF SCIENCE AND TECHNOLOGY** [SA/SA]; 4700 King Abdullah University of Science and Technology, Thuwal, 23955-6900 (SA).

(72) Inventors: **BISETTI, Fabrizio**; 4700 King Abdullah University of Science and Technology, Thuwal, 23955-6900 (SA). **SCRIBANO, Gianfranco**; 4700 King Abdullah University of Science and technology, Thuwal, 23955-6900 (SA).

(81) Designated States *(unless otherwise indicated, for every kind of national protection available)*: AE, AG, AL, AM, AO, AT, AU, AZ, BA, BB, BG, BH, BN, BR, BW, BY, BZ, CA, CH, CL, CN, CO, CR, CU, CZ, DE, DK, DM, DO, DZ, EC, EE, EG, ES, FI, GB, GD, GE, GH, GM, GT, HN, HR, HU, ID, IL, IN, IR, IS, JP, KE, KG, KN, KP, KR, KZ, LA, LC, LK, LR, LS, LU, LY, MA, MD, ME, MG, MK, MN, MW, MX, MY, MZ, NA, NG, NI, NO, NZ, OM, PA, PE, PG, PH, PL, PT, QA, RO, RS, RU, RW, SA, SC, SD, SE, SG, SK, SL, SM, ST, SV, SY, TH, TJ, TM, TN, TR, TT, TZ, UA, UG, US, UZ, VC, VN, ZA, ZM, ZW.

(84) Designated States *(unless otherwise indicated, for every kind of regional protection available)*: ARIPO (BW, GH, GM, KE, LR, LS, MW, MZ, NA, RW, SD, SL, ST, SZ, TZ, UG, ZM, ZW), Eurasian (AM, AZ, BY, KG, KZ, RU, TJ, TM), European (AL, AT, BE, BG, CH, CY, CZ, DE, DK, EE, ES, FI, FR, GB, GR, HR, HU, IE, IS, IT, LT, LU, LV, MC, MK, MT, NL, NO, PL, PT, RO, RS, SE, SI, SK, SM, TR), OAPI (BF, BJ, CF, CG, CI, CM, GA, GN, GQ, GW, KM, ML, MR, NE, SN, TD, TG).

Declarations under Rule 4.17:

— *as to applicant's entitlement to apply for and be granted a patent (Rule 4.17(ii))*

— *as to the applicant's entitlement to claim the priority of the earlier application (Rule 4.17(iii))*

Published:

— *with international search report (Art. 21(3))*

— *before the expiration of the time limit for amending the claims and to be republished in the event of receipt of amendments (Rule 48.2(h))*

(54) **Title**: DEVICES AND METHODS FOR GENERATING AN AEROSOL

(57) **Abstract**: Aerosol generators and methods of generating aerosols are provided. The aerosol can be generated at a stagnation interface between a hot, wet stream and a cold, dry stream. The aerosol has the benefit that the properties of the aerosol can be precisely controlled. The stagnation interface can be generated, for example, by the opposed flow of the hot stream and the cold stream. The aerosol generator and the aerosol generation methods are capable of producing aerosols with precise particle sizes and a narrow size distribution. The properties of the aerosol can be controlled by controlling one or more of the stream temperatures, the saturation level of the hot stream, and the flow times of the streams.

WO 2016/030750 A1

DEVICES AND METHODS FOR GENERATING AN AEROSOL

CROSS-REFERENCE TO RELATED APPLICATION

This application claims the benefit of and priority to U.S. Provisional Application Serial No. 62/041,323, having the title "DEVICES AND METHODS FOR GENERATING AN AEROSOL," filed on August 25, 2014, the disclosure of which is incorporated herein by reference in its entirety.

FIELD OF THE DISCLOSURE

This disclosure is generally in the field of methods and devices for generating aerosols, in particular liquid aerosols having a narrow size distribution.

BACKGROUND

The formation of particles from supersaturated vapor is a fundamental process in aerosol-laden flows in nature and technological applications. Examples in environmental flows include clouds and atmospheric aerosols. In the materials processing industry, the condensation of a precursor vapor (e.g. a metallic chloride) into monodisperse liquid droplets by mixing with a cold inert gas is a preliminary step in the production of advanced powders (Ingebrethsen *et al.*, *J. Colloid Interface Sci.,* 1983, 95(1):228-239; Kodas *et al.,* "Aerosol Processing of Materials", 1998, Wiley-VCH, New York).

In many of these situations, the vapor concentration and temperature fields are not homogeneous in space. For example, a hot vapor stream may combine with a cold gas in laminar or turbulent jets, wakes, or mixing layers. Local vapor super-saturation and droplet condensation therefore occur as a consequence of fluid, heat, and mass transport across mixing layers, which are thin compared to the largest scales of the flow. The nucleation and growth rates of particles are highly nonlinear and very sensitive to local temperature and vapor concentration. Thus, the yield and particle size distribution of the condensing particles depends critically on the coupling between the aerosol microphysical processes and heat and mass transport in the spatially inhomogeneous mixing field (Clement, *Proc. R.Soc. London A,* 1985, 398(1815):307-339; Nguyen *et al., J. Colloid Interface Sci.*, 1987, 119(2):491-504; Pesthy *et al.,* Journal of Colloid and Interface Science, 1983, 91(2):525–545).

A detailed theory of the formation of aerosols by condensation in inhomogeneous flows with heat and mass transfer has been developed mostly in the context of laminar flow

condensers. In a flow condenser, vapor flows through a tubular reactor where the temperature of the gas is lowered by conduction to the walls or by injection of a cold gas, causing the formation of particles (Nguyen *et al., J. Colloid Interface Sci.*, 1987, 119(2):491-504; Pesthy *et al.,* Journal of Colloid and Interface Science, 1983, 91(2):525–545). Alternative configurations include laminar coaxial jets (Brock *et al.,Exp. J. Aerosol Sci.,* 1986, 17(1):11-22) and gas-flow diffusion chambers (Anisimov *et al., J. Aerosol Sci.*, 1985, 16(2):97-107). In these experiments, reported values for the particle number density lie between 10^2 and 10^8 cm^{-3} and particle diameters are in the range 1 to 10 μm.

Numerical approaches for condensing aerosols with heat and mass transfer have been proposed in the literature (Pesthy et al., 1983; Phanse and Pratsinis, 1989; Pratsinis, 1988; Pyykönen and Jokiniemi, 2000). Pesthy (1983) and Pesthy et al. (1983) propose a detailed model for the aerosol phase and solve the general dynamic equation along each streamline in a condenser tube. They consider nucleation and growth processes only and neglect coagulation because the particle concentration is low. They repeat the calculations for the classical Becker-D¨oring and the Lothe-Pound nucleation theories (Springer, 1978), with the latter providing a better comparison with experiments. Pratsinis (1988) formulates a moment method with closure based on a lognormal particle size distribution. Nucleation, condensation, and coagulation processes are included, together with heat and mass coupling to the gas-phase. The method is applied successfully to the simulation of aerosol generation in a model laminar flow condenser tube (Phanse and Pratsinis, 1989). Pyyk¨onen and Jokiniemi (2000) develop and implement sectional approaches for the dynamics of aerosols in laminar flow condensers.

The opposed flow belongs to the broad category of Hiemenz-type stagnation flows (Wang, *Eur. J. Mech. B.-Fluid,* 2008, 27(6):678-683). In this type of opposed flow configuration there are two streams of fluid that flow one towards the other from opposite directions. When these two streams collide a stagnation plane or mixing layer is formed. Wang (2008) provides a formal description of the velocity field between the two opposed fluid flow nozzles. Wang (2008), however, does not provide any discussion of aerosols or other mass transport across the nozzles.

SUMMARY

Aerosol generators and methods of aerosol generation are provided that overcome the problems with traditional aerosol generation. For example, the aerosol generation and aerosol generation methods provided can produce aerosols with precisely controlled properties and size distributions that do not vary in time. The aerosol can be generated at a

stagnation plane where there exists an interface between a hot, wet stream and a cold, dry stream.

In some embodiments the aerosol generator has a first nozzle and a second nozzle oriented opposed to the first nozzle. In any one or more aspects, the first nozzle can contain or be in thermal contact with a heating unit, for example capable of a temperature range of about 20°C to about 300°C. The second nozzle can contain or be in thermal contact with a refrigerating unit, for example capable of a temperature range of about -50°C to about 20°C. The first nozzle can be a hot nozzle that can be in fluid contact with a vaporization unit for generating the vapor of a compound to be turned into an aerosol of liquid droplets. Although the aerosol generator can generally be of any size capable of generating the stagnation interface to produce the aerosol, in some embodiments the nozzles have a diameter of about 5 mm to about 3 cm. The distance between the nozzles can likewise be adjusted to control the aerosol properties. In some embodiments the distance between the nozzles is about 0.25-2 times the diameter of the nozzles.

Aerosols having controlled properties, including aerosols having a narrow size distribution, can be generated with the aerosol generators and aerosol generation methods described herein. The methods can, in some embodiments, use any one or more of the aerosol generators described herein. The methods can include generally providing a hot stream containing the vapor of a compound to be aerosolized, providing a cold stream opposed to the hot stream, and forming a stagnation plane at an interface between the hot and cold streams to form the aerosol comprising the compound. In any one or more aspects of the methods, the hot stream can have a temperature of about 20 - 300 ºC. The cold stream can have a temperature of about -50°C to about 20ºC. The hot stream, the cold stream, or both streams can have a velocity of about 30 cm s^{-1} to about 10 m s^{-1}.

In any one or more aspects of the embodiments, the hot stream can be operated at a maximum saturation ratio of unity (fully saturated), or less. In one or more aspects the saturation ratio can be 0.8. The minimum saturation ratio of the hot stream can be as small as desired. For example the saturation ratio can be 0.1, or less than 0.1.

In any one or more aspects of the embodiments, the aerosol generators and methods described herein can be used to make aerosols having a narrow size distribution. For example, the aerosols can have an average particle size of about 0.1-10 µm. One or more properties of the aerosol can be controlled by controlling the temperature of the hot stream, the temperature of the cold stream, the saturation level of the hot stream, the flow rate of the hot stream, the flow rate of the cold stream or any combination thereof.

Other devices, methods, features, and advantages of the present disclosure for generating an aerosol will be or become apparent to one with skill in the art upon examination of the following drawings and detailed description. It is intended that all such

additional systems, methods, features, and advantages be included within this description, be within the scope of the present disclosure, and be protected by the accompanying claims.

BRIEF DESCRIPTION OF THE DRAWINGS

Many aspects of the disclosure can be better understood with reference to the following drawings. The components in the drawings are not necessarily to scale, emphasis instead being placed upon clearly illustrating the principles of the present disclosure. Moreover, in the drawings, like reference numerals designate corresponding parts throughout the several views.

Fig. 1 is a diagram of a modeled two-dimensional axisymmetric flow configuration of an embodiment of the present disclosure having a cold inlet stream of nitrogen (bottom) mixing with a hot inlet stream of nitrogen with dibutyl phthalate (DPB) vapor (top), as an exemplary vapor of a chemical species having a low saturation vapor pressure. The fluids are introduced with equal uniform velocities u_0 from two opposed nozzles of infinite diameter separated by a distance $2L$.

Fig. 2A is a graph of the dimensionless velocity (left axis) and the dimensionless strain rate (right axis) as a function of the dimensionless axial coordinate. Fig. 2B is a graph of the normalized temperature (θ) and the dibutyl phthalate (DBP) mass fraction with (Y/Y_h) and without ($\bar{Y}/Y_h$) the contribution from vapor consumption. η=-1 indicates the cold inlet and η=1 indicates the hot inlet. The stagnation plane is at $\eta_0 \approx 0$. The flow parameters are u_0=0.5 ms-1, 2L=25 mm with T_h = 159 °C and S_h = 0.8 (Y_h=0.0194).

Fig. 3A is a graph of the nucleation rate J according to the Becker-Döring theory of homogeneous nucleation (on a logarithmic scale along the right axis) as a function of the mixture fraction. Fig. 3B is a graph of the condensation rate in the free molecular regime as a function of the mixture fraction (right axis). The saturation ratio (S) is plotted along the left axis in both figures. The rate expressions are reported both including (solid lines) and neglecting (dashed lines) the DBP vapor consumption. The flow parameters are u_0=0.5 ms-1, 2L=25 mm with T_h = 159 °C and S_h = 0.8 (Y_h=0.0194).

Fig. 4A is a graph of the number density N (cm^{-3}) along the left axis and the volume fraction (ppm) along the right axis as a function of the non-dimensional coordinate η=x/L. Fig. 4B is a graph of the count mean diameter d_{10} (μm) along the left axis and the polydispersity index (PDI) along the right axis as a function of the non-dimensional coordinate η=x/L. η=-1 indicates the cold inlet and η=1 indicates the hot inlet. The stagnation plane is at $\eta_0 \approx 0$.The flow parameters are u_0=0.5 ms-1, 2L=25 mm with T_h = 159 °C and S_h = 0.8 (Y_h=0.0194).

Fig. 5A is a graph of the domain averages number density (cm^{-3}) as a function of the flow time (ms) for various values of the saturation ratio. Fig. 5B is a graph of the domain averaged volume fraction (ppm) as a function of the flow time (ms) for various values of the saturation ratio. The values are reported including (thick lines) and neglecting (thin lines) the contributions from vapor consumption.

Fig. 6A is a graph of the maximum value of the saturation ratio as a function of the flow time (ms). Fig. 6B is a graph of the droplet mean diameter in the domain (μm) as a function of the flow time (ms). All flows have Re=310 and T_h=159 ºC.

Fig. 7A is a graph of the domain averaged number density (cm^{-3}) as a function of the flow time (ms) according to the Becker-Döring theory of homogenous nucleation (BD) and the self-consistent correction (SCC). Fig. 7B is a graph of the domain averaged volume fraction (ppm) as a function of the flow time (ms) according to the Becker-Döring theory of homogenous nucleation (BD) and the self-consistent correction (SCC). Values are plotted for values of S_h equal to 0.6, 0.8, and 1.0. All flows have Re = 310, T_h = 159 ºC, and T_c = 0 ºC.

Fig. 8A is a graph of the domain averaged number density (cm^{-3}) as a function of the flow time (ms) obtained with a mixture-average model of the mass diffusion coefficient of DBP (Le_{DBP}) and letting Le_{DBP} =1 (Le=1) for values of S_h equal to 0.6, 0.8, and 1.0. Fig. 8B is a graph of the maximum mean diameter (μm) as a function of the flow time (ms) obtained with a mixture-average model of the mass diffusion coefficient of DBP (Le_{DBP}) and letting Le_{DBP} =1 (Le=1) for values of S_h equal to 0.6, 0.8, and 1.0. All flows have Re=310, T_h = 159 ºC, and T_c = 0 ºC.

Fig. 9A is a graph of the normalized DBP mass fraction as a function of the mixture fraction for different values of the Lewis number of the condensing DBP vapor. Several isocontours of the saturation ration are also shown in dashed lines. Fig. 9B is a graph of the maximum value of the saturation ratio (left axis) and the maximum nucleation rate ($cm^{-3}s^{-1}$) (right axis) as a function of the Lewis number for values of S_h equal to 0.6, 0.8, and 1.0. All flows have Re=310, T_h = 159 ºC, and T_c = 0 ºC.

Fig. 10 is a schematic of an experimental aerosol generator containing a hot nozzle and an opposed cold nozzle for generating a stagnation plane between the nozzles.

Fig. 11A is a cut-off view of the opposed nozzles, the upper hot nozzle and the lower cold nozzle. Fig. 11B depicts a diagram of the flow of the opposed streams and the formation of the stagnation plane. Fig. 11C is a picture of the flow for condensation of dibutyl phthalate, as an exemplary chemical species having a low saturation vapor pressure, at the stagnation plane. The flow time in the example pictures is on the order of 10 ms. The upper stream has a temperature of 425 K and a DBP saturation ratio of 0.5. The lower stream has a temperature of 296 K.

Fig. 12 is a graph of the operating parameters as a function of the ratio between the distance between the nozzles (2L) and the nozzle diameter (D) along the left axis and the volumetric flow rate (slm) along the bottom axis for a nozzle diameter of 10 mm. On the same graph line as constant flow time and Reynolds number are reported.

Fig. 13 is a graph of the operating parameters as a function of the ratio between the distance between the nozzles (2L) and the nozzle diameter (D) along the left axis and the volumetric flow rate (slm) along the bottom axis for a nozzle diameter of 25 mm. On the same graph line as constant flow time and Reynolds number are reported.

Fig. 14 is a particle image velocimetry snapshot of the flow field between the two nozzles with the stagnation plane in the middle position relative to the two nozzles for 2L/D = 0.5 for a nozzle diameter of 10 mm.

Fig. 15 shows the radial profile of the axial velocity (m/s) at one of the nozzle outlets for three different flow rates for 2L/D=0.5 and a nozzle diameter of 10 mm.

Fig. 16 shows the radial profile of the radial velocity (m/s) at one of the nozzle outlets for three different flow rates for 2L/D =0.5 and a nozzle diameter of 10 mm.

Fig. 17 is a particle image velocimetry snapshot of the flow field between the two opposed nozzles with the stagnation plane in the middle position relative to the two nozzles for 2L/D = 1.0 for a nozzle diameter of 10 mm.

Fig. 18 shows the radial profile of the axial velocity (m/s) at one of the nozzle outlets for three different flow rates for 2L/D =1.0 and a nozzle diameter of 10 mm.

Fig. 19 shows the radial profile of the radial velocity (m/s) at one of the nozzle outlets for three different flow rates for 2L/D =1.0 and a nozzle diameter of 10 mm.

Fig. 20 is a particle image velocimetry snapshot of the flow field between the two opposed nozzles with the stagnation plane in the middle position relative to the two nozzles for for 2L/D = 2.0 for a nozzle diameter of 10 mm.

Fig. 21 shows the radial profile of the axial velocity (m/s) at one of the nozzle outlets for three different flow rates for 2L/D =2.0 and a nozzle diameter of 10 mm.

Fig. 22 shows the radial profile of the radial velocity (m/s) at one of the nozzle outlets for three different flow rates for 2L/D =2.0 and a nozzle diameter of 10 mm.

Fig. 23 depicts the axial velocity along the centerline between the opposed two nozzles, the axial velocity measured for four different separation distances between the nozzles.

Fig. 24 is a graph of the inverse of the flow time as a function of Reynolds number and separation distance between the two opposed nozzles.

Fig. 25 is a graph of the number density measured in a nucleation experiment as a function of the saturation ratio in the hot stream. All flows have
Re =700, T_H = 159 ºC, and T_C = 20 ºC.

Fig. 26 is a graph of the size distribution measured in an experiment as a function of the saturation ratio in the hot stream. All flows have Re = 700, T_H = 159 ºC, and T_C = 20 ºC.

DETAILED DESCRIPTION

The present disclosure provides aerosol generators and methods of aerosol generation that use an opposed flow configuration to generate an aerosol. Described below are various embodiments of the present devices and methods for generating an aerosol. Although particular embodiments are described, those embodiments are mere exemplary implementations of the system and method. One skilled in the art will recognize other embodiments are possible. All such embodiments are intended to fall within the scope of this disclosure. Moreover, all references cited herein are intended to be and are hereby incorporated by reference into this disclosure as if fully set forth herein. While the disclosure will now be described in reference to the above drawings, there is no intent to limit it to the embodiment or embodiments disclosed herein. On the contrary, the intent is to cover all alternatives, modifications and equivalents included within the spirit and scope of the disclosure.

I. AEROSOL GENERATOR

Aerosol generators are provided. In various aspects aerosol generators are provided that produce a narrowly distributed or “quasi-monodisperse” aerosol. In various aspects the aerosol can be monodisperse, meaning that the aerosol droplets all have substantially the same size. However, we use the term “monodisperse” more broadly herein, as defined below.

The aerosol generators include two or more nozzles spatially oriented in an opposed flow configuration. As used herein, two nozzles are said to be oriented in an opposed flow configuration when the nozzles are spatially oriented such that a fluid stream generated by one nozzle impinges upon the fluid stream generated by the other nozzle an angle of approximately 180° to create a stagnation plane. For example, the two streams can flow in completely parallel paths but in opposing direction. In some embodiments the paths of the streams are almost parallel, e.g. forming an angle of greater than about 160° greater than about 170°, greater than about 175°, greater than about 178°, or greater than about 179°. In some embodiments the flows are completely collinear, meaning that the streams are parallel with the central long axes of the streams collinear in space. The terms “stagnation plane” and “stagnation surface” are used interchangeably herein to refer to an imaginary plane or interface between opposed fluid streams where the velocity along the direction of stream flow is about zero.

Fig. 11A depicts a cut-off view of one embodiment of two nozzles (**100a** and **100b**) having an opposed flow configuration. The upper nozzle **100a** and the lower nozzle **100b** are spatially oriented such that a fluid stream generated by the upper nozzle **100a** and a fluid stream generated by the lower nozzle **100b** impinge in the stagnation region **110** between the tip of the upper nozzle **120a** and the tip of the lower nozzle **120b**. Each nozzle (**100a** and **100b**) has an inner nozzle (**130a** and **130b**), each creating an inner nozzle void (**140a** and **140b,** respectively) in fluid communication with the upper and lower nozzle tips (**120a** and **120b,** respectively). In one or more aspects the inner nozzles (**130a** and **130b**) are contoured, narrowing in inner diameter towards their respective nozzle tips (**120a** and **120b**). Second upper and lower nozzles (**150a** and **150b**, respectively) can be included that surround and are spaced apart from the inner upper and lower nozzles (**130a** and **130b**) such than annular spaces or voids (**160a** and **160b**) are provided between inner upper nozzle **130a** and second upper nozzle **150a**, and between inner lower nozzle **130b** and second lower nozzle **150b**, respectively. Each nozzle (**100a** and **100b**) further has an outer shield (**170a** and **170b**) surrounding and spaced apart from the second upper and lower nozzles (**150a** and **150b**), each outer shield creating an outer void or annular space (**180a** and **180b**) around the outside of the second upper and lower nozzles (**150a** and **150b**), respectively.

In one or more embodiments inner nozzle voids, **140a** and **140b**, provide fluid flow passageways or conduits through which the Main Streams N2a and N2b (**Fig. 10**) pass, exiting the upper and lower nozzle tips, **120a** and **120b**. Annular spaces **160a** and **160b** also provide passageways or conduits for fluid flow, for example Co-flow Streams N2a and N2b (**Fig. 10**). Nozzles **100a** and **100b** can be configured such that the Main Streams and Co-flow Streams pass through the nozzles in the same direction exiting nozzle-tips 120a and 120b, respectively. The Co-flow Streams can, thus, serve as curtains for the Main Streams shielding the Main Streams from the external environment once the Main Streams exit their nozzle tips.

The outer shields, **170a** and **170b**, can facilitate controlling the temperature of the nozzles, and in particular the temperature of one or both fluid Co-flow Streams or the temperature of one or both of the fluid Co-flow Streams and one or both of the fluid Main Streams. For example, the outer void **180a** of the upper nozzle **100a** can contain a heating fluid in fluid communication with a heating unit that maintains the heating fluid at a specific hot temperature. The heating fluid in the outer void **180a** is in thermal contact with annular space **160a**, thereby regulating the temperature of a fluid passing there through. The heating fluid can also be in indirect thermal contact with the inner nozzle **130a**, thereby regulating the temperature of a fluid passing through the inner void **140a**. Further, the outer void **180b** of the lower nozzle **100b** can contain a cooling fluid in fluid communication with a

refrigerating unit that maintains the cooling fluid at a specific cold temperature. The cooling fluid in the outer void **180b** is in thermal contact with annular space **160b** and can also be in thermal contact indirectly with the inner nozzle **130b**. The cooling fluid can thereby regulate the temperature of a fluid passing through annular space **160b**, or regulate the temperature of fluids passing through both the annular space **160b** and the inner void **140b**. One skilled in the art will recognize, however, that the heating and cooling of the fluid streams can be reversed such that upper nozzle **100a** is cooled and lower nozzle **100b** is heated.

The nozzle tips can be separated by any distance as long as the streams generated form a stagnation interface. In some embodiments the distance between the nozzle tips will be from about 1-100 mm, 1-60 mm, 2-60 mm, 5-50 mm, 5-40 mm, 5-30 mm, 5-25 mm, or 5-20 mm, among others. In some embodiments the distance between the nozzle tips is measured as a multiple of the diameter of the nozzle tip. For example, the distance between the nozzle tips can be between about 0.125-4 times, 0.25-4 times, 0.25-3 times, 0.25-2 times, 0.5-2 times, or 1-2 times the diameter of the nozzle tips among others. The diameter of the nozzle tips can generally be, for example, about 1-100 mm, 1-60 mm, 2-60 mm, 3-60 mm, 3-40 mm, 4-40 mm, 5-40 mm, 7-35 mm, or 10-25 mm, among others.

The aerosol generator will generally contain additional components to, among other things, provide the carrier streams, regulate the temperature, and/or vaporize the compound to form the aerosol. **Fig. 10** is a schematic of one embodiment of an aerosol generator. The carrier streams are provided by nitrogen gas sources, although in general any inert gas can be used. For example, the carrier gas could be nitrogen, argon, helium, or other gasses. The carrier gas can be introduced as Main Stream N2a and Main Stream N2b for the upper nozzle **100a** and the lower nozzle **100b**, respectively. The system can include dryers and filters to dry and clean the carrier gas in either or both streams.

Either one or both of the carrier gas streams can include mass flow controllers (MFCs) and pressure regulators to control the flow and pressure of the carrier gases within the nozzles. This can be used, for example, to control the flow rate of the streams exiting the nozzles and the flow time or residence time of the aerosol particles in the generator. The flow rate can generally be adjusted to any value to obtain the desired aerosol properties and rate of generation of the aerosol. In some embodiments, for example, the flow rate of the carrier streams is about 10- 30,000 $cm^3 s^{-1}$, 10-20,000 $cm^3 s^{-1}$, 10-10,000 $cm^3 s^{-1}$, 20-10,000 $cm^3 s^{-1}$, 30-10,000 $cm^3 s^{-1}$, 30-5,000 $cm^3 s^{-1}$, 30-2,000 $cm^3 s^{-1}$, 100-2,000 $cm^3 s^{-1}$, 500-2,000 $cm^3 s^{-1}$, or 500-1,500 $cm^3 s^{-1}$, among others. The velocity can vary between about 10 cm s^{-1} – 15 m s^{-1}, 20 cm s^{-1} - 15 m s^{-1}, 30 cm s^{-1} – 10 m s^{-1}, among others. The flow time or residence time may generally be from about 0.01 to 1,000 ms, among others. Here we are using the terms “flow time” and “residence time” interchangeably.

The aerosol generator can have a refrigerating unit to cool a fluid or refrigerant used to control the cold temperature of the cold nozzle **100b**. The cold temperature can be generally any temperature between the freezing temperature of the carrier and the hot temperature of the hot nozzle **100a**. For example, among others, the refrigerating unit can have a temperature range of about -100-100ºC, -50-100 ºC, -50-50 ºC, -50-20°C, -20-50 ºC, -20-40 ºC, -10-40 ºC, -10-30 ºC, 0-30 ºC, or 0-20 ºC. The aerosol generator can likewise have a heating unit such as a hot oil circulating unit to control the hot temperature of the hot nozzle **100a**. The heating unit can generally have any temperature between the temperature of the cold nozzle 100b and the degradation temperature, i.e. the temperature at which the carrier gas or the compound to be turned into an aerosol degrade, i.e. undergo decomposition. In some embodiments the heating unit will have a temperature range of about 20-500 ºC, 20-500 ºC, 20-400 ºC, 20-300 ºC, 20-250 ºC, 20-200 ºC, or 20-150 ºC among others. The temperature of the hot stream will generally be hot enough to vaporize or to aide in vaporizing a compound to be aerosolized. The heating fluid and the cooling fluid can be introduced in the outer voids **180a** or **180b**, respectively. The Co-flow Streams can also be dried, filtered, metered and according to the nozzle where they will go heated or cooled. In one or more aspects, the Co-flow Streams have the same temperature as the Main Stream they are shielding.

The aerosol generator can contain a vaporization unit used to vaporize the one or more compounds that will be aerosolized. The compounds to be aerosolized can be, for example, introduced through a syringe pump into the vaporization unit or into the hot stream. For example Main Stream N2a. The compounds to be aerosolized, or vaporized, are described below. In one or more aspects, the compounds can be any chemical species having a low saturation vapor pressure.

II. METHODS OF GENERATING AN AEROSOL

Methods of generating an aerosol at the stagnation interface between a hot, wet stream and a cold, dry stream are provided. The methods can generally be applied with any suitable device. However, in some embodiments the methods are applied using aerosol generators as describe above. The methods provided are useful for generating liquid aerosols, and especially for generating monodisperse liquid aerosols that are stable over time. An aerosol is said to be stable over time if one or more of the properties of the aerosol do not fluctuate by more than 20%, 15%, 10%, 5%, 3%, 2%, or 1% over a period of time of about 1 s, 10 s, 20 s, 30 s, 1 minute, 2 minutes, 3 minutes, or 10 minutes, and for even 2-3 hours, or more. The properties of the aerosol that do not fluctuate over time can include, among others, the average particle size, the span, the coefficient of variation, the polydispersity index, the aerosol number density, and the flow rate.

The methods can be used to generate aerosols having any particle size. For example, the particle size can be about 0.1-100 μm, about 0.1-50 μm, about 0.1-10 μm, about 0.5-10 μm, about 1-10 μm, or about 2-5 μm. The aerosols can have a narrow size distribution. The size distribution can be quasi-monodisperse, or preferably monodisperse. For example, in some embodiments the particles in the aerosol have a span less than about 5, 4, 3, 2, 1, or 0.5. In some embodiments the particles in the aerosol have a COV of about 1.0 or less, about 0.5 or less, about 0.4 or less, or about 0.3 or less. A monodisperse collection of particles can be a collection of particles wherein about 40% or more, about 50% or more, about 60% or more, about 70% or more, or about 80% or more of the particles have a particle size that is within ± 400 nm, ± 200 nm, ± 100nm, ± 10 nm, ± 8 nm, ± 6 nm, ± 5 nm, or ± 3 nm of the average particle size. In one aspect, among others, the COV can be in the range 0.3 – 0.4, and the SPAN can be in the range 0.7 – 1. As a non-limiting example, the saturation ratio can be 0.1 and the particle size distribution can be:

+/- 400 nm 90% of particles

+/- 100 nm 40% of particles

+/- 50 nm 20% of particles

+/- 10 nm 6% of particles

In another aspect, the saturation ratio can be 0.24, and the particle size distribution can be:

+/- 400 nm 55% of particles

+/- 100 nm 15% of particles

+/- 50 nm 8% of particles

+/- 10 nm 2% of particles

The compound to be vaporized can generally be any compound capable of being vaporized in the hot stream. In some embodiments the compound is an inorganic compound. The compound can also be an organic compound. The compound will generally have a boiling point of less than about 600 ºC, less than about 500 ºC, less than about 400 ºC, less than about 350 ºC, less than about 325 ºC, or less than about 300 ºC. The compound can be any molecule weight, although in some embodiments the compound is a small molecule. The term “small molecule”, as used herein, generally refers to an organic molecule that is less than about 2000 g/mol in molecular weight, less than about 1500 g/mol, less than about 1000 g/mol, less than about 800 g/mol, or less than about 500 g/mol. Small molecules are non-polymeric and/or non-oligomeric. For example, the compound can have a molecular weight of less than about 400 g/mol, less than about 350 g/mol, or less than about 300 g/mol. In one embodiment, the compound can be dibutyl phthalate (DBP), though one skilled in the art will recognize other compounds can be used to generate the aerosol. In some embodiments the method includes providing 1, 2, 3, 4, or more different compounds to be

aerosolized. This allows for generating aerosols having a wide variety of chemical compositions.

The methods can include any method of generating a stagnation plane between opposed fluid streams having a first, hot, humid/wet stream and a second, cold, dry stream. In some embodiments the method includes providing a hot stream containing a vapor of a compound to be aerosolized, providing a cold stream opposed to the hot stream, and forming a stagnation plane at an interface between the hot stream and the cold stream to form an aerosol of the compound. Typically the vapor of the compound(s) to be aerosolized is added to the hot stream. A stream is said to be wet when the saturation level of the vapor in the stream is greater than about 0.1, 0.7, 0.8, 0.9, or 0.95.

The present methods and device for aerosol generation provide considerable flexibility over aerosol generation. For example, the number of aerosol droplets formed, their density, sizes and size distribution can all be controlled. Thus it is possible to generate a specific number of aerosol particles of a specific size. Any one or more of the separation distance between the opposed nozzles, the diameter of the nozzles, the flow rates of the hot and cold Main Streams through the nozzles, the concentration or saturation ratio of the compound to be aerosolized or vaporized in its hot carrier gas stream and the temperatures of the hot and cold Main Streams can be controlled to control aerosol generation. The separation distance between the nozzles, nozzle diameters and hot and cold stream flow rates all effect the “flow time” of the compound vapor in the stagnation interface between the opposed nozzles and the amount of time for aerosol droplet formation. For example, decreasing separation distance between the opposed nozzles can decrease flow time. Everything else remaining constant, a decrease of separation distance by ½ can decrease flow time by ½. In general, aerosol droplet size increases with an increase in flow time and vice versa. The saturation ratio of the compound to be aerosolized can be controlled by controlling the metering of the compound into the hot stream. In general, more aerosol nucleation occurs the colder the temperature of the cold stream.

III. USES OF THE AEROSOLS

The aerosols, aerosol generators, and methods of generating aerosols can be used in a variety of applications. The aerosol generators can be used as micro-reactors. For example, US Patent No. 7,811,543 to Didenko *et al.,* the contents of which are incorporated herein by reference, describes the synthesis of nanoparticles and other nanometer sized materials by pyrolysis of aerosols. The pyrolysis can include mixing the aerosol with oxygen to make the stream combustible prior to passing the aerosol through the flame. The aerosol generator can be used to generate liquid nanoparticles for filter testing, as a first step for nanoparticle production (see, for example, US Patent 5,525,320), aerosol research needing

monodisperse particles, and for production of nanoparticles to be used in electronic, semiconductor industries, material industries.

IV. DEFINITIONS

The terms "particle size" and “particle diameter”, as used interchangeably herein, mean simply the geometrical diameter of a sphere as indicated below. The term "average particle size" and “average particle diameter” mean the number average of the particle sizes of a collection of particles. When we talk about diameter, we mean simply the geometrical diameter of a sphere, as all droplets (for those sizes <= 10 micron) are spherical in shape.

The “span” for a distribution of particles can be computed from the formula

$$Span = \frac{D_{v0.9} - D_{v0.1}}{D_{v0.5}};$$

where $D_{v0.1}$, $D_{v0.5}$, and $D_{v0.9}$ are defined such that 10%, 50%, and 90% of the particles in the collection of particles have a dimension smaller than $D_{v0.1}$, $D_{v0.5}$, and $D_{v0.9}$ respectively.

The coefficient of variation (COV) for a collection of particles is the standard deviation of particle sizes divided (normalized) by the average particle size.

The terms “quasi-monodisperse” and “monodisperse”, as used herein, characterize a collection of particles where the particle size scatter is within a narrow range of sizes. The collection of particles can be a collection of particles having a span of about 2 or less, about 1 or less, about 0.8 or less, or about 0.5 or less. The collection of particles can be a collection of particles having a COV of about 0.5 or less, about 0.4 or less, or about 0.3 or less. The collection of particles can be a collection of particles wherein about 40% or more, about 50% or more, about 60% or more, about 70% or more, or about 80% or more of the particles have a particle size that is within ± 400 nm, ± 200 nm, ± 100 nm, ± 10 nm, ± 8 nm, ± 6 nm, ± 5 nm, or ± 3 nm of the average particle size for the collection of particles. In any one or more aspects the COV, SPAN and particle size distributions can include those described above.

Where a range of values is provided, it is understood that each intervening value, to the tenth of the unit of the lower limit unless the context dictates otherwise, between the upper and lower limit of that range and any other stated or intervening value in that stated range, is encompassed within the disclosure. The upper and lower limits of these smaller ranges may independently be included in the smaller ranges and are also encompassed within the disclosure, subject to any specifically excluded limit in the stated range. Where the

stated range includes one or both of the limits, ranges excluding either or both are also included in the disclosure.

Ratios, concentrations, amounts, and other numerical data may be expressed in a range format. It is to be understood that such a range format is used for convenience and brevity, and should be interpreted in a flexible manner to include not only the numerical values explicitly recited as the limits of the range, but also to include all the individual numerical values or sub-ranges encompassed within that range as if each numerical value and sub-range is explicitly recited. To illustrate, a concentration range of "about 0.1% to about 5%" should be interpreted to include not only the explicitly recited concentration of about 0.1 % to about 5 %, but also include individual concentrations (e.g., 1%, 2%, 3%, and 4%) and the sub-ranges (*e.g.*, 0.5%, 1.1%, 2.2%, 3.3%, and 4.4%) within the indicated range. In an embodiment, the term "about" can include traditional rounding according to significant figure of the numerical value. In addition, the phrase "about 'x' to 'y'" includes "about 'x' to about 'y'".

Unless defined otherwise, all technical and scientific terms used have the same meaning as commonly understood by one of ordinary skill in the art to which this disclosure belongs. Although any methods and materials similar or equivalent to those described can also be used in the practice or testing of the present disclosure, the preferred methods and materials are now described.

All publications and patents cited in this specification are incorporated by reference as if each individual publication or patent were specifically and individually indicated to be incorporated by reference and are incorporated by reference to disclose and describe the methods and/or materials in connection with which the publications are cited. The citation of any publication is for its disclosure prior to the filing date and should not be construed as an admission that the present disclosure is not entitled to antedate such publication by prior disclosure. Further, the dates of publication provided could differ from the actual publication dates that may need to be independently confirmed.

As will be apparent to those of skill in the art upon reading this disclosure, each of the individual embodiments described and illustrated has discrete components and features which may be readily separated from or combined with the features of any of the other several embodiments without departing from the scope or spirit of the present disclosure. Any recited method can be carried out in the order of events recited or in any other order logically possible.

Embodiments of the present disclosure will employ, unless otherwise indicated, techniques of molecular biology, microbiology, nanotechnology, organic chemistry, biochemistry, botany, which are within the skill of the art. Such techniques are explained fully in the literature.

EXAMPLES

Now having described various embodiments of the present disclosure the following Examples describe some additional embodiments of the present disclosure. While embodiments of the present disclosure are described in connection with the following examples and the corresponding text and figure, there is no intent to limit embodiments of the present disclosure to this description. The intent is to cover all alternatives, modifications, and equivalents within the spirit and scope of embodiments of the present disclosure.

The Examples below describe results from numerical simulations of an opposed flow model and the development of an experimental aerosol generator for studying the effects of various hydrodynamic mixing parameters on the aerosol nucleation and growth. Additional details of the numerical simulations can be found in Appendices A-D. Additional details of the experimental aerosol generation can be found in Appendices E-H.

Effects of hydrodynamic mixing on nucleation and growth of condensation aerosols

Configuration, methods, and models

The geometry of the flow considered is shown in **Fig. 1**. The configuration is two-dimensional and axisymmetric. The fluid is introduced with uniform and equal velocity u_0 from two nozzles of infinite diameter separated by a distance $2L$. Let x be the axial coordinate placed along the axis of the geometry and r be the radial coordinate normal to it.

Cold, dry nitrogen flows from the bottom and mixes with hot nitrogen laden dibutyl phthalate (DBP) vapor issuing from the top. Condensation of the vapor into liquid droplets occurs inside the mixing layer. DBP is chosen as a model vapor due to the numerous experimental and numerical results available (Lesniewski *et al.*, *Proc. Royal Soc. London* A, 1998, 454(1977):2477; Nguyen *et al., J. Colloid Interface Sci.,* 1987, 119(2):491-504; Pesthy *et al.*, *J. Colloid Interface Sci.,* 1983, 91(2):525–545;Phanse *et al., Aerosol Sci. Tech.,* 1989, 11(2):100-119) and its low vapor pressure at near ambient temperature. The modeling approach for the flow field and scalar transport is adapted from Kee et al. (*Proc. Combust. Inst.*, 1989, 22(1): 1479–1494) and extended to include the simulation of droplet nucleation and growth with a method of moments and a quadrature-based closure McGraw (1997, Aerosol Science and Technology, 27(2):255–265).

Flow field and scalars transport

Following Kee et al., it is assumed that a stream function ψ(x, r) describes the flow field:

$$\psi(x,r) = r^2 U(x), \tag{1}$$

where the axial and radial velocity components u and v are related to U(x) by

$$\rho u = \frac{1}{r}\frac{\partial \psi}{\partial r} = 2U \quad \text{and} \quad \rho v = -\frac{1}{r}\frac{\partial \psi}{\partial x} = -r\frac{dU}{dx} \tag{2}$$

and the density ρ is modeled with the ideal gas equation of state $\rho = p/R_{N2}\,T$. R_{N2} is the gas constant for molecular nitrogen. The effect of vapor and droplets on the gas density is neglected due to the low concentration of DBP.

Within this framework, the steady-state equations for mass, axial, and radial momentum reduce to a single equation for U(x):

$$\frac{d}{dx}\left[\mu\frac{d}{dx}\left(\frac{G}{\rho}\right)\right] - 2\frac{d}{dx}\left(\frac{UG}{\rho}\right) + \frac{3}{\rho}G^2 + H_p = 0, \tag{3}$$

where

$$G = \frac{dU}{dx} \tag{4}$$

μ is the dynamic viscosity of the gas mixture, and H_p is the radial pressure gradient eigenvalue (Chapman *et al.*, 1975, Applied Scientific Research, 31(3):223–239, Kee et al. (*Proc. Combust. Inst.*, 1989, 22(1): 1479–1494)), which is a parameter computed as part of the solution.

All scalar fields, including temperature, DBP mass fraction, and aerosol moments, are assumed to depend only on the axial coordinate *x*. The transport equations for temperature and DBP mass fraction are:

$$2UC_p\frac{dT}{dx} - \frac{d}{dx}\left(\lambda\frac{dT}{dx}\right) = 0 \tag{5}$$

and

$$2U\frac{\partial Y}{\partial x} - \frac{\partial}{\partial x}\left(\rho D\frac{\partial Y}{\partial x}\right) - \dot{\omega} = 0 \tag{6}$$

In the equations above, the specific heat of the mixture C_p is constant and *D* is the binary diffusion coefficient of DBP in molecular nitrogen. It is assumed that the temperature of the mixture is not affected by nucleation and vapor condensation due to the low mass fraction of DBP, which remains below 2.5×10^{-2} throughout the domain for all conditions considered. The term $\dot{\omega}$ in Eq. (6) represents a negative contribution to Y due to nucleation and condensation removing DBP molecules from the gas phase. Thus, the velocity and

temperature fields are independent of aerosol processes, but the DBP mass fraction *Y* is not.

In the present work, the effect of buoyancy on the momentum and scalar transport is neglected. The relative importance of natural and forced convection may be estimated from the ratio of the Grashof number and the square of the Reynolds number $Gr/Re^2 \propto g(\Delta T)L/(u^2_0 T)$, where *g* is the gravitational acceleration, *T* is a representative mean temperature, and ΔT is the temperature difference between the hot and cold streams. Thus, buoyancy effects may become important for large nozzle separation 2*L* and low inlet velocities u_0.

Aerosol dynamics

The method of moments is used to solve for the aerosol dynamics. The *k*-th moment of the particle size distribution n(x; ξ) is defined as:

$$\mu_k = \int_0^\infty \xi^k n(x;\xi) d\xi \quad , \qquad (7)$$

where ξ represents the diameter of a spherical particle. The steady transport equation for μk is

$$\frac{\partial}{\partial x}(u\mu_k) - \frac{\partial F_d^k}{\partial x} - S_k = 0 \qquad (8)$$

The source term Sk in Eq. (8) reflects the aerosol's internal processes according to equation

$$S_k = \int_0^\infty \dot{S}(x;\xi)\xi^k d\xi = J_k + G_k + C_k \quad , \qquad (9)$$

representing the contribution of homogeneous nucleation (J_k), droplet growth by condensation (G_k), and coagulation (C_k). The diffusion term in Eq. (8) has the following form:

$$F_d^k = \int_0^\infty D_p(x;\xi)\frac{\partial}{\partial x}\left(\xi^k n(x;\xi)\right) d\xi \quad , \qquad (10)$$

where Dp is the diffusion coefficient of droplets with diameter ξ.

In this work, the effect of gravity on the evolution of the aerosol is not considered due to the small size of the particles and their negligible settling velocity compared to the reference velocity of the flow configuration. The Quadrature Method of Moments (QMOM) (McGraw, 1997) is used to close the source S_k and diffusion F_d^k terms. The particle size distribution (PSD) is assumed to be of the form:

$$n(x;\xi) = \sum_{i=1}^{N} W_i(x)\delta\left(\xi - \zeta_i(x)\right) \quad , \qquad (11)$$

where N Dirac delta functions are placed at ζ_i (the abscissas) and weighted by W_i (the weights) with i = 1,...,N. Based on the QMOM closure, the source terms in Eq. (9) are expressed as (Marchisio and Fox, 2005; Marchisio et al., 2003):

$$J_k = J d_{\mathrm{cr}}^{k}, \qquad (12)$$

$$G_k = k\sum_{i=1}^{N} W_i \zeta_i^{k-1} G(\zeta_i) \quad , \qquad (13)$$

$$C_k = \frac{1}{2}\sum_{i=1}^{N}\sum_{j=1}^{N}\left(\zeta_i^3 + \zeta_j^3\right)^{k/3}\beta(\zeta_i,\zeta_j)W_iW_j - \sum_{i=1}^{N}\sum_{j=1}^{N}\zeta_i^k\beta(\zeta_i,\zeta_j)W_iW_j \quad , \qquad (14)$$

where J and d_{cr} are the homogeneous nucleation rate and the corresponding critical diameter at which nucleation occurs. G and β are the growth rate and the coagulation kernel of droplets, respectively.

The expression for the diffusion flux in Eq. (10) may be expanded as

$$F_{\mathrm{d}}^{k} = \overline{(D_p)}_k \frac{\partial \mu_k}{\partial x} + \mu_k\left(\frac{\partial \overline{(D_p)}_k}{\partial x} - \overline{\left(\frac{\partial D_p}{\partial x}\right)}_k\right) \quad , \qquad (15)$$

where the average of a scalar function ϕ weighted by the kth moment is

$$\overline{\phi_k} \equiv \frac{1}{\mu_k}\int_0^{\infty}\phi(\xi)\xi^k n(x;\xi)d\xi \quad . \qquad (16)$$

For simplicity, the second term in Eq. (15) is neglected and

$$F_{\mathrm{d}}^{k} = \overline{(D_p)}_k \frac{\partial \mu_k}{\partial x} \quad . \qquad (17)$$

Boundary conditions and solution methodology

The one-dimensional domain of length 2L extends from the bottom nozzle at x=−L to the top nozzle at x=L. At the hot and cold inlets, the temperature, DBP vapor mass fraction, and velocities are prescribed:

$T = T_h$, $Y = Y_h$, $U = -\rho_h u_0/2$, $G=0$ at $x=L$, (18)

$T = T_c$, $Y = Y_c$, $U = \rho_c u_0/2$, $G=0$ at $x=-L$, (19)

where $T_h > T_c$ and $Y_c = 0$. Note that the axial velocity is u_0 at both inlets and the boundary conditions $G(x = \pm L) = 0$ are equivalent to setting the radial velocity to zero by virtue of continuity. Boundary conditions for the DBP vapor mass fraction are such that the cold stream is dry, i.e. $Y(x = -L)=0$,and the hot stream is laden with DBP vapor: $Y(x=L)=Y_h$ with saturation ratio S_h. The boundary conditions for the moments at $x = \pm L$ are set assuming that the inlet PSD consists of monodisperse droplets with a diameter equal to 2.3 nm, which corresponds to the critical size for the saturation ratios and temperatures considered in this study. The droplet number density at the inlets is set to a low value equal to 1 m^{-3}.

The solution methodology is as follows. Firstly, the equations for momentum (Eq. (3)) and temperature (Eq. (5)) are solved together as a boundary value problem with the radial pressure gradient eigenvalue H_p as parameter (see Eq. (3)). The equations are reformulated into a system of first order ordinary differential equations (ODEs) and the MATLAB™ function bvp4c is used to obtain the solution. bvp4c implements the fourth-order three-stage Lobatto IIIa formula for first order boundary value problems with a parameter.

Secondly, the unsteady form of the equations for the DBP mass fraction (Eq. (6)) and the aerosol moments (Eq. (8)) are integrated in time with an in-house FORTRAN code using the BDF stiff solver CVODE in the SUNDIALS suite (Hindmarsh *et al., ACM Trans. On Mathematical Software,* 2005, 31(3):363-396) until a steady solution is achieved. Since the velocity and temperature fields obtained from bvp4c are independent of the aerosol's moments and the DBP mass fraction, they are left unchanged during the time integration with CVODE.

The convective fluxes in Eq. (6) and Eq. (8) are evaluated using a second- order upwind scheme. The diffusive flux in Eq. (6) is discretized with a second- order central difference formula. The domain is discretized with 600 points and the mesh is refined near the stagnation plane. The finest mesh spacing at the stagnation plane is such that $\Delta\eta = 3.3\times10^{-6}$ with $\eta = x/L$. The solution on the finest grid (600 points) was found to be identical to the solution on a grid featuring 300 points and mesh spacings twice as large.

In order to enhance the robustness of the numerical approach, the evolution equations for the logarithm of the aerosol moments are solved as part of the ODE system. This transformation preserves the positivity of the moments in a convenient and straightforward fashion

In this work, N = 2 Dirac deltas are employed, requiring the transport of 4 moments of the PSD: μ_0, μ_1, μ_2, *and* μ_3. The Product Difference (PD) algorithm (Gordon, *J. of Math. Phys.*, 1968, 9:655) is used for the inversion of the transported moments into the corresponding abscissas and weights. As the moments are transported in space and evolve according to the aerosol's internal processes, they must satisfy the Stieltjes conditions in

order to guarantee the existence of the PSD. Violation of these conditions causes the PD algorithm to fail (McGraw, 2012; Wright, 2007).

Results and discussion

In the opposed flow configuration, the Reynolds number Re = u_0L/v is defined based on the inlet velocity u_0, half the nozzle separation distance L, and the kinematic viscosity v, here evaluated for molecular nitrogen at 80 °C. The global strain rate $a = u_0/L$ is the inverse of a reference flow time scale τ and is used to parameterize the response of the aerosol to varying mixing rates. In this work, L and u_0 are varied over a range of values in order to change a, while keeping the Reynolds number constant (Re = 310). Because the Reynolds number is constant, all flows considered here are hydrodynamically self-similar, which facilitates the analysis.

The temperature of the cold stream T_c is kept at either 0 or 23 °C, while the hot stream temperature T_h is constant at 159 °C. At the hot inlet, the DBP vapor concentration is varied, achieving saturation ratios between 0.6 and 1 and corresponding mass fractions between 0.0145 and 0.024. The inlet stream conditions selected in the present numerical study are accessible experimentally, since they feature viable temperatures and saturation ratios in the hot stream, and ambient or near ambient temperatures at the cold inlet.

The nozzle separation distance and inlet velocity vary in the ranges $0.125 \leq 2L \leq 16\text{cm}$ and $0.08 \leq u_0 \leq 10\text{ms}^{-1}$, resulting in $0.05 \leq \tau \leq 10^3$ ms. Such a wide range of conditions is explored numerically for the purpose of documenting the aerosol response over a wide range of flow times.

Nonetheless, separation distances and inlet velocities at either end of the range may be impractical to realize experimentally. For example, small flow times of the order of 0.1 ms require separation distances of the order of 1 mm and inlet velocities of 10 ms^{-1}. Conversely, large flow times of the order of 100 ms require separation distances of 5 cm and inlet velocities of 0.5 ms^{-1}. While small separation distances are likely to result in significant heat transfer to the nozzles and complicate aerosol sampling, large separation distances will result in flows dominated by buoyancy and instabilities. From an experimental point of view, a much narrower range of inlet conditions yielding flow times $1 \leq \tau \leq 10$ ms is most relevant.

Overview of the flow and aerosol fields

Fig. 2A shows the velocity u and strain du/dx as a function of x, all quantities made non-dimensional by u_0 and L. The cold inlet lies at $\eta = x/L = -1$ and the hot inlet is at $\eta = 1$. Although the results in **Fig. 2** are shown for selected inlet conditions, they are representative of all flow fields considered in this work due to hydrodynamic self-similarity and the small range of variation in temperature boundary conditions. Changes in the global strain rate $a = u_0/L$, while holding $u_0L \propto \text{Re} = \text{const}$, simply rescale the velocity u and coordinate x by constant factors: one the inverse of the other.

In **Fig. 2A**, the two cases shown differ solely in the temperature of the cold stream (T = 0 or 23 °C), while all other parameters are equal. In the range of values of T_c considered, the variation of the density field in response to a change in the temperature of the cold stream has a very limited effect on the hydrodynamics of the flow. This secondary effect may be neglected in the discussion of the response of aerosol properties to varying stream conditions.

The normalized temperature $\theta = (T - T_c)/(T_h - T_c)$ and DBP mass fraction Y/Y_h vary across the domain and establish a mixing layer as shown in Fig. 2B. Both fields increase monotonically from zero (cold stream) to unity (hot stream) and display an inflection point near the stagnation plane. Since the effect of vapor condensation on temperature is negligible, the normalized temperature θ is a conserved scalar and is equivalent to the mixture fraction ϕ. The ratio between the domain length L and the mixing layer thickness $\delta = 1/\max\{d\phi/dx\}$ scales as $\delta/L \propto (ReS_c)^{-1/2}$, where S_c is the Schmidt number of the scalar under consideration, and is constant in the present study (not shown).

The DBP mass fraction Y/Y_h is not a conserved scalar, unless vapor consumption by the aerosol phase is negligible (see Fig. 2(b)). In the same figure, it is also apparent that the maximum gradient of Y/Y_h near the stagnation plane is considerably larger than that of θ due to the mass diffusion coefficient of DBP being less than the thermal diffusion coefficient, as reflected by the Lewis number of DBP: $Le = D_{th}/D \approx 4.6$.

The rate of nucleation and condensation-based growth are shown in Fig. 3 alongside the saturation ratio S as a function of mixture fraction ϕ. Results obtained both including and neglecting the consumption of DBP vapor ($\dot{\omega} = 0$ in Eq. (6)) are illustrated. Due to the nonlinear dependence of the saturation pressure Ps on temperature, the saturation ratio $S \propto Y/Ps$ peaks on the cold side of the stagnation plane for $\phi < 0.5$, despite the fact that the mass fraction of DBP vapor is maximum on the hot side. The nucleation rate displays a maximum on the cold side of the mixing layer also, even though the peak is closer to the stagnation plane than the peak in saturation ratio owing to sensitivity to temperature. In the range of stream conditions considered in this work, the peak nucleation rate varies greatly between $O(10^2)$ and $O(10^{11})$ $cm^{-3}s^{-1}$.

As shown in **Fig. 3A**, the nucleation rate is very sensitive to the local mixture composition and temperature, and vapor consumption has an important effect on nucleation rate. The nucleation rate decreases by several orders of magnitude if vapor depletion by the aerosol phase is considered in the equations. As will be shown, the sensitivity of the nucleation rate to vapor depletion has important implications for aerosol quantities and their response to the strain rate a.

In **Fig. 3B**, the growth rate of droplets in the free molecular regime is shown as a function of mixture fraction ϕ. The peak condensation-based growth rate varies between 810 and 1600 μm s^{-1} for all conditions considered. Unlike the nucleation rate, the condensation growth rate peaks on the hot side of the stagnation plane at $\phi \approx 0.8$ and is less sensitive to the local mixture composition and temperature. As a result, condensation does not vary appreciably in response to vapor depletion as shown in **Fig. 3B**. At the location of peak growth, the saturation ratio is greater than unity but much lower than peak saturation, indicating that, across the mixing layer, a hot and mildly supersaturated mixture is most conducive to growth, while a colder and highly supersaturated mixture leads to the most intense nucleation.

The spatial distribution of the number density, volume fraction, and count mean diameter of the DBP aerosol across the mixing layer are shown in **Fig. 4**. Starting from the cold side, where nucleation is most intense, the number density increases rapidly near the stagnation plane, where it reaches its peak value. The number density drops sharply on the hot side of the mixing layer across the stagnation plane, where mixture temperature and DBP concentrations are not favorable to nucleation.

For all conditions considered in this work, aerosol particles populate a very narrow region of the domain. In **Fig. 4A**, this region extends across $\Delta\eta = 0.05$, which corresponds to 2.5% of the separation distance between the nozzles. The non-dimensional extent of the region where aerosol particles are abundant is related functionally to the normalized width of the mixing layer δ/L, which decreases as $Re^{-1/2}$. Owing to the dependence of the source terms of the aerosol moments on the temperature and vapor mass fraction, the width of the aerosol layer is of the same order as that of the mixing layer of the scalars. In this study, the Reynolds number is held constant, so that the ratio between the mixing layer width and the nozzle separation is constant for all flows.

The volume fraction *f* peaks at the stagnation plane, where large number densities and long flow times encourage sustained droplet growth by condensation. Like the number density, the aerosol volume fraction is distributed across the stagnation plane, but displays a sharper and narrower profile. This narrower profile reflects the fact that the volume fraction increases at a faster rate than the number density due to the enhancement brought by both the nucleation of new particles and the increase in surface density of the existing particles during growth.

In this study, the peak volume fraction ranges between $O(10^{-6})$ and $O(10^{2})$ ppm, depending on flow and stream parameters. The peak value of the number density ranges between $O(10^{7})$ and $O(10^{14})$ cm^{-3}. For these relatively low values of number density, coagulation rates are negligibly small.

The count mean diameter of the aerosol particles $d_{10} \equiv \mu 1/\mu 0$ is at a maximum at the stagnation plane, while smaller particles populate regions of the domain further away from the stagnation plane (see **Fig. 4(B)**). The spatial distribution of the polydispersity index (PDI), defined as $w \equiv d_{30}/d_{10} = \mu_0^{2/3}\mu_1^{-1}\mu_3^{1/3}$ (Friedlander, "Smoke, dust and haze: fundamental of aerosol dynamics" in Topics in Chemical Engineering, 2000, Oxford University Press), is also shown in **Fig. 4B**. The PDI indicates that the droplets are nearly monodisperse at the stagnation plane and more polydisperse further away from it near the region where they nucleate, in accordance with the observations of Pratsinis (1988). The spatial distribution of the PDI reflects the dependence of the particle's growth rate on size. In the free molecular regime, which extends up to particles 0.1 μm in diameter, the particles' condensation-based growth rate is independent of size. As particles grow bigger, they enter the transitional and continuum regimes, where growth rates decrease for increasing droplet size. Thus, provided enough time is given for the aerosol to evolve, small particles catch up in size with larger ones, leading to a narrowing of the size distribution and a nearly monodisperse population of droplets near the stagnation plane. This mechanism is not unique to the present configuration, but rather is typical of most aerosols formed by condensation and is readily exploited to generate nearly monodisperse product aerosols by condensation (Pratsinis, 1988).

Hydrodynamic effects on aerosol growth

In order to assess the dependence of the condensing aerosol on the hydrodynamic mixing time scale, the flow time τ, defined as the inverse of the strain rate $a = u_0/L$, is varied parametrically between 0.05 and 10^3 ms while keeping Re = 310. The response of the aerosol is observed in terms of the domain averaged number density

$$N_L = \frac{1}{2L}\int_{-L}^{L} N(x)dx \tag{20}$$

and volume fraction

$$f_L = \frac{1}{2L}\int_{-L}^{L} f(x)dx \tag{21}$$

The results are shown in **Fig. 5** for various values of saturation in the hot stream S_h and for two cold stream temperatures, T = 0 and 23 °C. At low values of $\tau = a^{-1}$, the domain averaged number density N_L increases with increasing τ, while the trend is opposite for large values of τ, and N_L displays a maximum for $\tau = \tau_{max}$ (see **Fig. 5A**). While the actual value of the number density varies depending on the stream conditions, the same behavior is apparent for all cases considered, regardless of the cold stream temperature and the vapor saturation ratio at the hot stream inlet.

For a given flow time τ, a decrease in the cold stream temperature or an increase in the vapor saturation ratio in the hot stream lead to significantly higher values of N_L, reflecting an increase in homogeneous nucleation rates. Within the limited range of saturation ratios considered ($0.6 \leq S \leq 1$) and with the small variation in cold stream temperature, the domain averaged number density N_L varies over more than seven orders of magnitude for flow times between 0.1 and 100 ms. The flow time at peak number density, τmax, shifts to lower values with increasing saturation ratios.

In **Fig. 5B**, the domain averaged volume fraction f_L is seen to increase rapidly with τ for small values of the flow time or high value of the strain rate. Like the number density, f_L increases with decreasing cold stream temperature and increasing hot stream vapor saturation for a given value of flow time τ. Unlike number density, however, f_L continues increasing with τ for large values of the flow time, albeit at a much slower rate, until the effect f increasing flow times on f_L saturates. Based on the results shown in **Fig. 5**, it is clear that N_L has a complex dependence on the flow time τ at given stream conditions and that this interaction is responsible for the non-monotonic behavior of N_L with τ, affecting f_L also. For small flow times $\tau \ll \tau_{max}$, i.e. for large inlet velocities u_0 and short separation distances L, both N_L and f_L increase with increasing τ and a longer flow time implies more time for the droplets to nucleate and grow. In particular, while N_L increases linearly with τ, f_L increases at a faster rate due to the enhancement in growth rates brought by increasing surface density. Furthermore, increasing values of saturation ratio at the hot stream inlet correspond to increasing values of N_L and f_L alike.

In contrast to the behavior at short flow times, at long flow times $\tau \gg \tau_{max}$, an increase in τ leads to decreasing number density N_L as well as the saturation of the volume fraction f_L. A related effect is that both the number density and volume fraction become significantly less responsive to changes in the hot stream saturation ratio for long flow times. In other words, at large values of the flow times, the increase in domain averaged number density N_L and volume fraction f_L due to increased saturation ratios across the domain is much less than at low values of the flow time. As will be explained below, this behavior is due to an important interaction between the DBP vapor spatial distribution, vapor consumption by the growing aerosol, and the peak saturation ratio in the domain.

In an effort to investigate the non-monotonic response of N_L to τ, the same calculations were repeated setting the source term $\omega^{\cdot} = 0$ in Eq. (6), thereby neglecting consumption of DBP vapor. It is worth mentioning that, for all conditions, condensation is responsible for most of the conversion of vapor DBP to liquid droplets. Nucleation controls the number density of droplets, but the contribution of nucleation to volume growth is negligible owing to the small size of the nucleating particles. In **Fig. 5**, it is shown that vapor consumption is negligible for very short flow times ($\tau \ll \tau_{max}$) as the results obtained when

vapor consumption is neglected overlap with those obtained with all terms in Eq. (6). At larger values of the flow time ($\tau \gg \tau_{max}$), the solution obtained when vapor consumption is neglected greatly surpasses the actual values of the number density and volume fraction.

The behavior observed in **Fig. 5** may be explained as follows. At longer flow times, condensation of vapor onto the surface of existing droplets results in the consumption of DBP vapor, which in turn suppresses nucleation and leads to a decrease in the domain-averaged number density N_L. This mechanism is quantified in **Fig. 6A**, where it is shown that, for all hot stream saturation ratios considered, large τ values lead to a decrease of the peak saturation ratio S_{max} in the domain, while S_{max} is constant for small values of τ . It is apparent that, as the peak saturation ratio increases, vapor scavenging manifests itself at shorter hydrodynamic times. For $S_{max} \geq 1000$, flow times in excess of 1 ms ($a \leq 10^{-3}$ s^{-1}) result in significant vapor consumption. If τ is sufficiently large, S_{max} becomes independent of the vapor saturation ratio at the hot inlet and the number density does not increase in response to increasing saturation at the hot inlet. Similar observations have been made by Brock et al. (1986) in a laminar coaxial jet experiment, where it is shown that an increase in the number, density and condensation rate depletes vapor and suppresses nucleation ("vapor scavenging"). The effect of vapor scavenging by condensation has been addressed by Pratsinis (1988) in a numerical simulation of a flow-tube condenser.

Considering the response of the aerosol to variations in flow time, we may define two regimes: the "nucleation" and the "condensation" regime. In the former, vapor consumption is negligible and the aerosol number density and volume fraction increase with increasing flow time, while in the latter, vapor consumption due to condensation is important, the number density decreases with increasing flow time and the volume fraction saturates. The transition between the two regimes occurs for flow time τ between 1 and 10 ms for the stream conditions considered, which lead to peak saturation ratios between 800 and 1300.

Fig. 6B shows the maximum mean diameter in the domain, occurring at the stagnation plane. The maximum mean diameter increases with flow time τ and, for all stream conditions and flow times considered, d_{max} lies between 0.5 and 10 μm. The rate of increase of d_{max} with flow time is highest at low values of τ and drops for increasing d_{max}, reflecting the fact that droplets transition from the free molecular growth regime into the continuum regime around 0.1 μm. Once the transition occurs, the growth rate decreases with size. The maximum mean diameter d_{max} is relatively insensitive to the cold stream temperature or the hot stream saturation ratio, being most sensitive to the flow time τ instead.

These results and the range of mean diameters observed are consistent with various studies on condensing aerosols (Brock et al., 1986; Pesthy et al., 1983) and suggest that it may be possible to control the number density and particle size of the

product aerosol independently by adjusting the saturation ratio in the hot stream S_h and the flow time τ.

Sensitivity of the solution to nucleation & transport models

The results presented so far rely on the Becker-Doring theory of homogeneous nucleation to describe the nucleation rate of DBP droplets. It is well known that homogeneous nucleation theories provide approximate values of nucleation rates, which are often found to over- or under-estimate experimental results considerably. Thus, it is appropriate to explore the dependence of the results on the nucleation model.

The self-consistent correction to the rate of homogeneous nucleation from an ideal supersaturated vapor proposed by Girshick and Chiu (*J. Chem. Phys.,* 1990, 93:1273) is implemented and the aerosol response investigated. Detailed expressions for the nucleation rate based on both theories are provided in Appendix A.

Fig. 7 shows the domain averaged number density as a function of the flow time τ for the same stream conditions explored previously and shown in **Fig. 5**. The overall trends of N_L are the same for the two theories. However, the solution based on the SCC theory of homogeneous nucleation yields a significantly higher N_L, which surpasses that obtained with the Becker-Doring theory by approximately two orders of magnitude for the same conditions. Moreover, the peak value of N_L shifts towards smaller values of τ. This behavior reflects the significantly higher values of the nucleation rate predicted by the SCC (Girshick *et al*, 1990) theory as compared to the classic Becker-Doring theory.

The ratio of the N_L,max values obtained in the two sets of calculations is approximately constant across all hot stream saturation ratios considered, as shown in **Fig. 7A**. This finding is consistent with the SCC expression for the nucleation rate, whereby a factor of the form $\exp(\Theta)/S$ appears in front of the classical Becker-Doring expression, where Θ is a dimensionless, temperature-dependent surface tension. Under most conditions, the range of Sh values considered is insufficient to introduce a strong dependence of the SCC correction factor on stream conditions.

Fig. 7B shows that, at small values of the flow time, the volume fraction also varies within one to three orders of magnitude in response to a change in the nucleation model. By contrast, the sensitivity of the domain averaged volume fraction f_L to the nucleation model is more limited at larger flow times ($\tau \gg 10$ ms), due to the saturation effect connected with vapor consumption.

From the data presented in **Fig. 7**, we may conclude that our results for the response of the aerosol to varying flow times and stream conditions are genuine features of the flow system, while the actual values of the number density vary within one to two orders of magnitude, depending on the nucleation model. This predicament is somewhat common to studies on condensing aerosols in both homogeneous and inhomogeneous flows, where the

sensitivity of the nucleation rate to models and gas-phase conditions produces a significant degree of uncertainty with regard to the results of detailed simulations (Pratsinis, 1998) and complicates the comparison with experiments.

The nucleation and growth rates in the domain depend on the local values of the DBP mass fraction and temperature. Both of these affect the saturation ratio, which is a controlling quantity in the expressions for nucleation and droplet growth rates. It is clear the spatial distribution of the DBP mass fraction depends on the balance of the convective and diffusive fluxes, as well as on the vapor consumption term (see Eq. 6). Compared to the thermal diffusion coefficient associated with heat transfer, DBP has a small mass diffusion coefficient, due to the relatively large size of the DBP molecule. The ratio $D_{th}/D = Le$ is approximately equal to 4.6, where D is the mass diffusion coefficient of DBP vapor in molecular nitrogen and $D_{th} = \lambda/\rho Cp$ is the thermal diffusion coefficient. As discussed in the commentary on **Fig. 2B**, a consequence of $Le \gg 1$ is that the DBP mass fraction gradient at the stagnation plane is significantly steeper than temperature gradient.

In **Fig. 8**, the implications of the diffusive flux model for DBP on the prediction of aerosol quantities are explored by letting Le = 1. The approximation $Le = D_{th}/D = 1$ is frequently adopted in the simplified treatment of mass transport in reactive flows and is usually referred to as the “unity Lewis number” approach (Poinsot and Veynante, 2005). **Fig. 8A** shows that, as the Lewis number of the condensing vapor is set equal to one, the number density N_L increases sharply. The change is significant, as the number density increases by three orders of magnitude in response to Le = 1. Furthermore, N_L,max shifts to smaller values of the flow time τ. Nonetheless, the overall behavior of N_L with respect to τ is unchanged. The changes are consistent with an increase in saturation ratio and associated nucleation rates for the Le = 1 case. The effect of the DBP mass flux model on the mean droplet diameter is shown in Fig. 8B, where it is apparent that the increase in number density at Le = 1 is accompanied by a moderate increase in droplet size for the same flow time τ. This trend is consistent with increased values of the saturation ratio for the unity Lewis number case.

The mechanism responsible for increasing the saturation ratio across the domain in response to a decrease in Lewis number of the vapor species is illustrated in Fig. 9A. The plot in **Fig. 9A** portrays the functional relation between the normalized DBP mass fraction Y/Y_h and the mixture fraction ϕ for various values of the DBP Lewis number. For the sake of simplicity, the functional relation is computed based on the analytical solution for passive scalars in a thin mixing layer (Chapman *et al.*, 1975). Also shown on the ϕ –Y/Y_h plane are isocontours of saturation ratio S from 1 to 10^5. Fig. 9A shows clearly that, as Le decreases, higher saturation ratios are accessible and are obtained across the mixing layer. **Fig. 9B**

illustrates the mechanism further and shows that minute variations in the mass diffusion coefficient of the condensing vapor result in remarkably large changes in the peak value of the saturation ratio S_{max} and nucleation rate J_{max}. The importance of vapor mass transport and related effects on the aerosol yield have been discussed in detail by Clement (1985).

The maximum domain averaged number density $N_{L,max}$ and flow time at peak number density τ_{max} as a function of the hot inlet saturation ratio S_h are shown for various models in **Fig. 10**. Recall that τ_{max} marks the transition from the nucleation to the condensation regime. It is clear that, depending on the models adopted, $N_{L,max}$ varies across four orders of magnitude, and that the variation due to the models is more important than the variation due to S_h. The latter is responsible for variations within one order of magnitude for saturation ratios between 0.5 and 1. Overall, peak mean number densities are in the range 10^3 to 10^9 cm^{-3}. Similarly, τ_{max} varies between 0.1 and 10 ms, i.e. over two orders of magnitude, for all cases and models considered and decreases sharply for increasing S_h, as expected. The results discussed above and shown in **Figs. 7** to **10** have important implications. Firstly, it is apparent that the quantitative predictions of the aerosol yield in non-homogeneous laminar flows with heat and mass transfer are very sensitive to the details of the homogeneous nucleation and diffusive mass flux model for the condensing vapor. This sensitivity should be considered when interpreting and evaluating the results of detailed calculations. With regard to mass transfer models in the context of closures for turbulent mixing, Lewis numbers other than unity are not often considered for the various species.

Secondly, it is widely accepted that molecular diffusion plays a secondary role in the rates of heat and mass transfer for high-Reynolds number flows. In fact, in the limit of infinitely large Reynolds number, turbulent mixing is independent of the molecular properties. Thus, one expects the details of DBP molecular mixing to become less important for increasing Reynolds number, so that turbulent aerosols of condensing vapor should behave as if the Lewis number were unity, even though this effect may not be apparent at the low and moderate Reynolds numbers accessible to numerical simulations and experiments. This limiting behavior is readily exploited in the formulation of RANS and LES closures, where unity Lewis number is assumed (Rigopoulos, 2010).

Conclusions

In this work, we have considered the formation and growth of aerosol particles from heat and mass transfer across a mixing layer in a canonical stagnation flow. The mixing layer is established between a cold/dry stream and a hot/humid stream laden with dibutyl phthalate vapor flowing from opposite directions. We assembled a detailed model for the transport of momentum, energy, vapor mass fraction, and aerosol moments in spatially

inhomogeneous flows. The response of the condensing aerosol to varying flow conditions, including stream temperatures, vapor concentration, inflow velocity, and distance between the inlets, was investigated.

We have shown that aerosol particles nucleate on the cold side of the mixing layer and that the largest particles populate a very narrow region at the stagnation plane, where, due to condensation-based growth, they become nearly monodisperse with diameters ranging from 0.1 to 10 μm, depending on the flow parameters.

Exploiting the dependence of the flow time on the inlet velocity and nozzle separation distance, the responses of number density, volume fraction, and mean particle diameter to varying mixing rates are characterized uniquely and two distinct aerosol regimes are identified. At low values of the flow time, or in the limit of fast mixing and low flow time, vapor scavenging by the aerosol phase is negligible (nucleation regime) and increasing flow times result in increasing particle concentrations in the aerosol phase. Conversely, at high values of the flow time, or in the limit of slow mixing, increasing flow times result in decreasing particle concentrations (condensation regime) due to the increased effect of vapor consumption. The mean droplet diameter and aerosol volume fraction increase monotonically with flow time. While the actual values of the aerosol properties depend on the saturation ratio in the hot stream, the qualitative trends are general. Finally, we have explored the sensitivity of our results to the homogeneous nucleation theory adopted, and to the details of mass transport for the condensing vapor. This analysis reveals that the actual values of number density and volume fraction change sharply as the models change. Nonetheless, the response of the aerosol remains qualitatively the same.

Development of an experimental flow configuration for aerosol generation

The experimental set up had two opposed jets with the same momentum flux, such that a stagnation plane forms between the two nozzles. A schematic of the instrumental setup is depicted in **Fig. 10**. The nozzles are oriented as depicted in **Fig. 11A**. The upper stream is hot nitrogen with DBP vapor and the lower is dry cold nitrogen. DBP droplets nucleate near the stagnation plane between the nozzles where the hot stream mixes with the cold one. A diagram of the model flow from this configuration is depicted in **Fig. 11B**, and a picture of the flow is shown in **Fig. 11C**. A thin layer of droplets is visible near the stagnation plane, located in the center of the region between the nozzles. The thin layer has a round shape because of an exhaust system active on the surround of the upper nozzle, used during the experiment to evacuate the liquid droplets formed during the nucleation experiment.

For the counter-flow with diameter of 10 mm an operation map is shown in **Fig. 12**, on the x-axis is reported the flow rate and on the y-axis is shown the separation over

diameter ratio. On **Fig. 12** three different Re numbers and flow times are shown. The flow time and Reynolds number are calculated by the following equations:

$\tau = L / U$, where U is the average velocity at the nozzle outlet and L is half of the separation distance between the two nozzles.

$Re = U L / (\nu)$, where ν is the kinematic viscosity of the fluid.

The curve with label $Gr/Re^2 = 0.1$ is the limit for buoyancy effect. The operating map shows the practical flow time for which it is possible to operate the counter-flow given a nozzle diameter, a flow rate, and a separation distance 2L.

An operating map for nozzle with diameter of 25 mm is shown in **Fig. 13**. In this case, it is possible to run the experiment with lower flow time compared with the case of diameter 10 mm.

When the velocity of the two streams, flowing through the two nozzles, is the same the stagnation plane is located in the middle zone between the two nozzles as it can be seen in **Figs. 14**, **17**, and **20**, which shown the flow field between the two nozzles for three separation between the two nozzles. For instance the stream issuing from the lower nozzle moves towards the upper nozzle. Near the middle zone the stream is diverted by the presence of the stream issuing from the upper nozzle. Two streams moving on the left and right direction are created. **Figs. 15**, **18**, and **21** show the axial velocity, velocity oriented parallel to the nozzle axis, along the diameter of the nozzles for three separation distances between the nozzles and three different values of the flow rates. These profiles have been measured close to the nozzle outlets. For instance, at the same separation, distance an increment in the flow rate will increase the value of the axial velocity. Changes in the profiles are visible when the separation is varied. **Figs. 16**, **19**, and **22** show the radial velocity, velocity oriented perpendicular to the nozzle axis, along the diameter of the nozzles for three separation distances between the nozzles and three different values of the flow rates. These profiles have been measured close to the nozzle outlets. For large separation between the nozzles the value of the radial velocity is around zero. Reducing the separation distance between the nozzles will increase the absolute value of the radial velocity. The maximum of the absolute value of the radial velocity is located near the coordinate r/R = +/-1. These profiles show the typical velocity field in counter-flow set-up.

Fig. 23 shows the axial velocity along the centerline for 4 separations. The non-dimensional axial coordinate is reported on the x-axis whereas the ratio between the local axial velocity and the mean velocity at the nozzle outlet is reported on the y-axis. -1 and 1 are the location of the nozzle outlets. Moving from x coordinate -1 to the right the velocity decreases to reach a zero value at the stagnation plane. The same behavior is observed when starting from x coordinate 1 and moving towards the left for the absolute value of the

velocity. The velocity profile changes when the separation between the two nozzles changes due to change in the pressure field generated in the region between the two nozzles.

In **Fig. 24** the inverse of the flow time is reported as a function of Reynolds number and the separation over diameter ratio. It is clear from this plot that it is possible to change linearly the inverse of the flow time by changing the Reynolds number when working for a given separation over diameter ratio. It means that it is possible to change in a controlled way the flow time by changing the flow rate from the nozzles.

In **Fig. 25** the number density of DBP liquid droplets measured during an experiment is reported as a function of the saturation level in the hot stream. The symbols are some measured values whereas the red line is a line connecting the mean values of the number density for that specific saturation level. The number density increases when the saturation level increased for the specific range of values tested.

The size distributions for some of the saturation level tested are reported in **Fig. 26**. The size is reported on the x-axis and the ratio between the number of droplets measured with a given size divided by the total number of droplets measured is reported on the y-axis. The size distribution shows that for low saturation level the peak of the size is located at small diameter. Increasing the saturation level the peak shift towards larger value of size. For the conditions analyzed the polydispersity index (PDI) is in the range 1.08 – 1.12.

The experimental set-up used in this work is suitable to study the nucleation and growth of droplets as a function of a single parameter in a well-controlled environment. This feature is related to the absence of foreign walls and surfaces.

It should be emphasized that the above-described embodiments of the present disclosure are merely possible examples of implementations, and are set forth only for a clear understanding of the principles of the disclosure. Many variations and modifications may be made to the above-described embodiments of the disclosure without departing substantially from the spirit and principles of the disclosure. All such modifications and variations are included within this disclosure.

We claim:

1. An aerosol generator comprising:
a first nozzle comprising a refrigerating unit,
a second nozzle comprising a heating unit and oriented opposed to the first nozzle, and
a vaporization unit in fluid communication with the second nozzle.

2. The aerosol generator of claim 1, wherein each of the nozzles have a diameter of about 5 mm to about 3 cm.

3. The aerosol generator of claim 1 or claim 2, wherein the refrigerating unit has a temperature range of about -50°C to about 20°C.

4. The aerosol generator of any one of claims 1-3, wherein the heating unit has a temperature range of about 20- 300 ºC.

5. The aerosol generator of any one of claims 1-4, wherein the nozzles are separated by a distance between about 1/4 the diameter of the nozzles and about twice the diameter of the nozzles.

6. The aerosol generator of any one of claims 1-5, wherein the aerosol generator is configured to provide flow rates through the first and second nozzles in the range of 10 cm s^{-1} to 15 m s^{-1}.

7. A method of generating an aerosol comprising:
providing a hot stream comprising a vapor of a compound,
providing a cold stream opposed to the hot stream, and
forming a stagnation plane at an interface between the hot stream and the cold stream to form the aerosol comprising the compound.

8. The method of claim 7, wherein the hot stream has a temperature of about 20-300 ºC.

9. The method of claim 7 or claim 8, wherein the cold stream has a temperature of about -50°C to about 20ºC.

10. The method of any one of claims 7-9, wherein the hot stream, the cold stream, or both streams have a velocity of about 30 cm s^{-1} to about 10 m s^{-1}.

11. The method of any one of claims 7-10, wherein the saturation ratio of the vapor in the hot stream is greater than about 0.1.

12. The method of any one of claims 7-11, wherein the aerosol has an average particle size of about 0.1-10 μm.

13. The method of any one of claims 7-12, wherein the aerosol has a monodisperse size distribution.

14. The method of claims 7-13, wherein one or more properties of the aerosol are controlled by controlling the temperature of the hot stream, the temperature of the cold stream, the saturation level of the hot stream, the flow rate of the hot stream, the flow rate of the cold stream or any combination thereof.

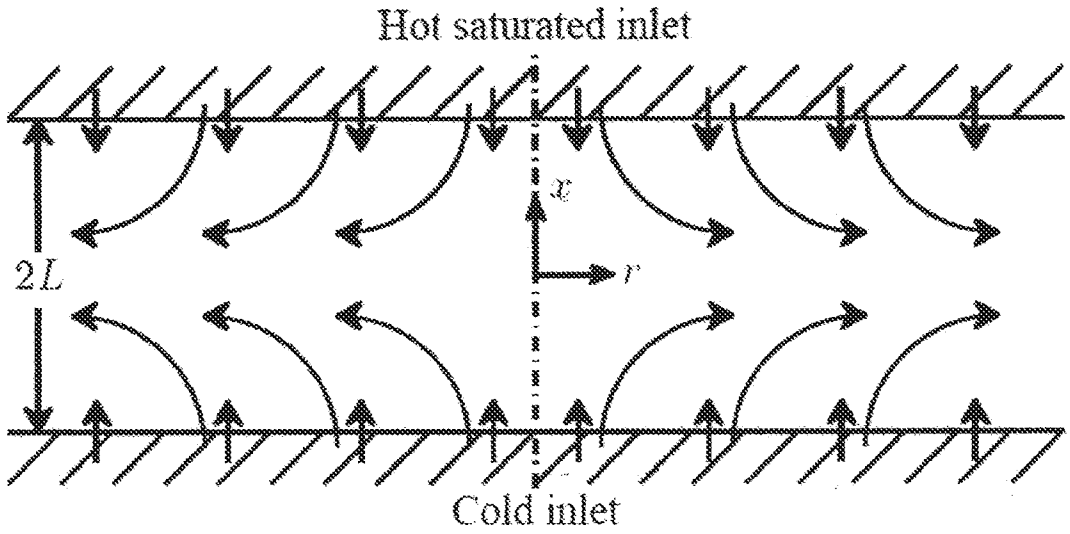

FIG. 1

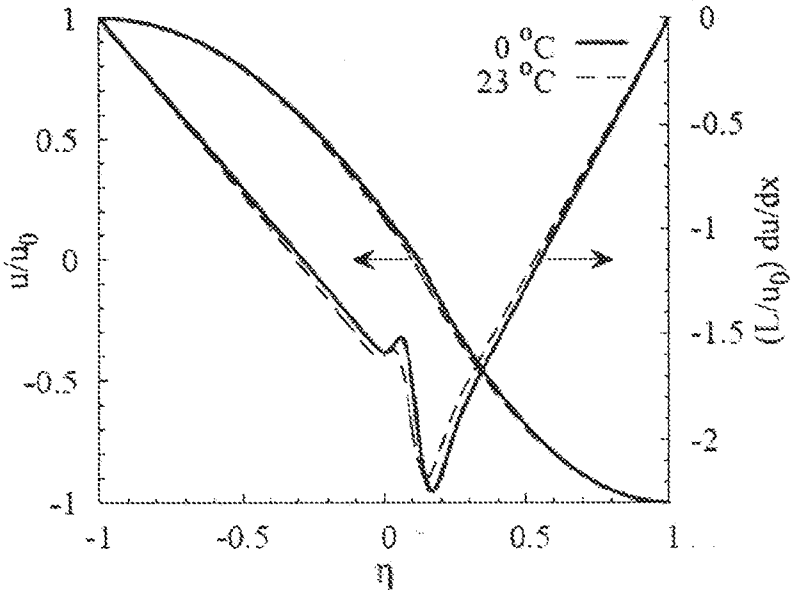

FIG. 2A

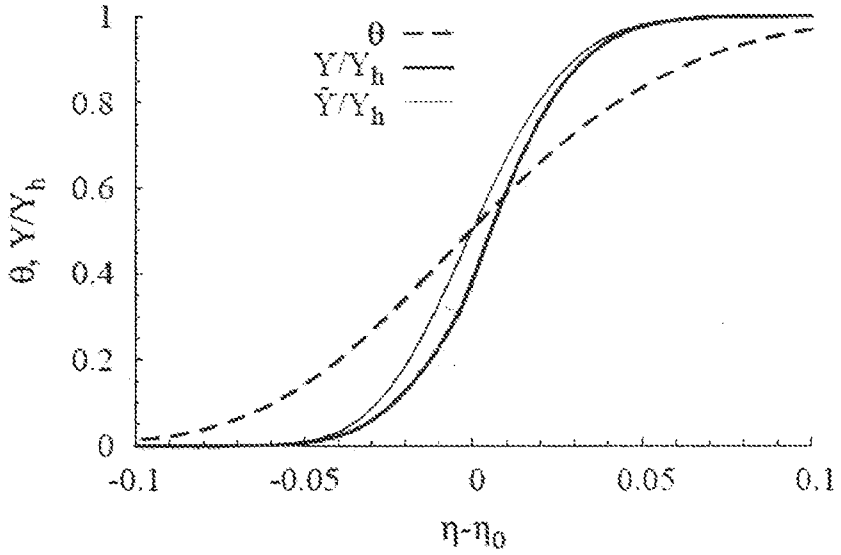

FIG. 2B

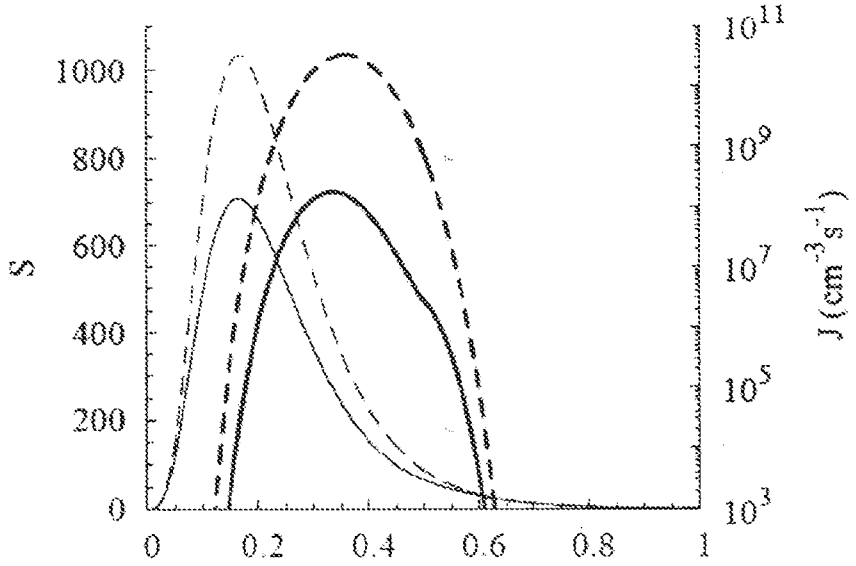
S
J (cm^{-3}s^{-1})
1000
800
600
400
200
0
10^{11}
10^{9}
10^{7}
10^{5}
10^{3}
0
0.2
0.4
0.6
0.8
1

FIG. 3A

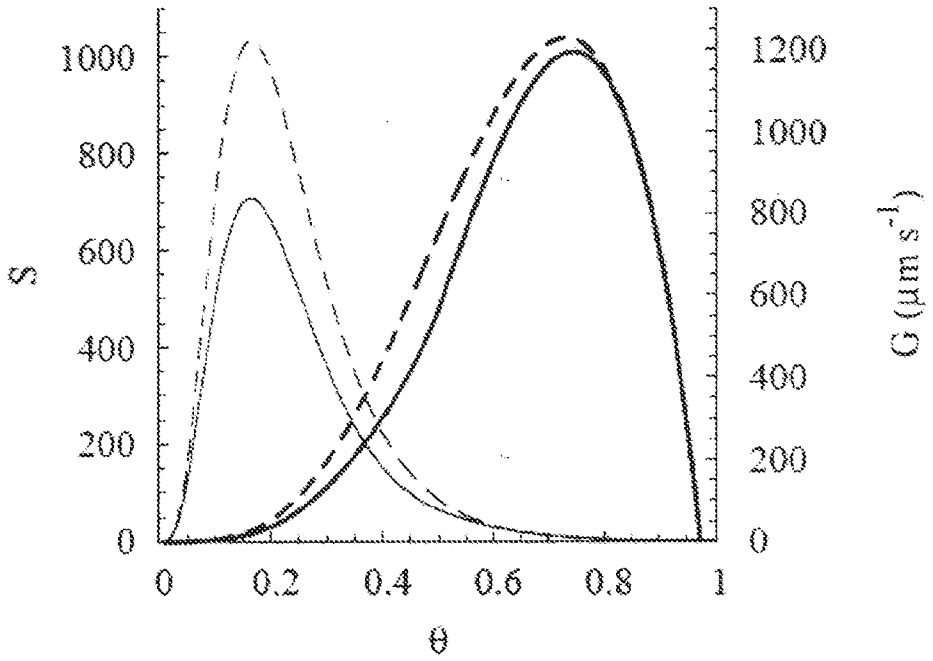
S
G (μm s^{-1})
1000
800
600
400
200
0
1200
1000
800
600
400
200
0
0
0.2
0.4
0.6
0.8
1
θ

FIG. 3B

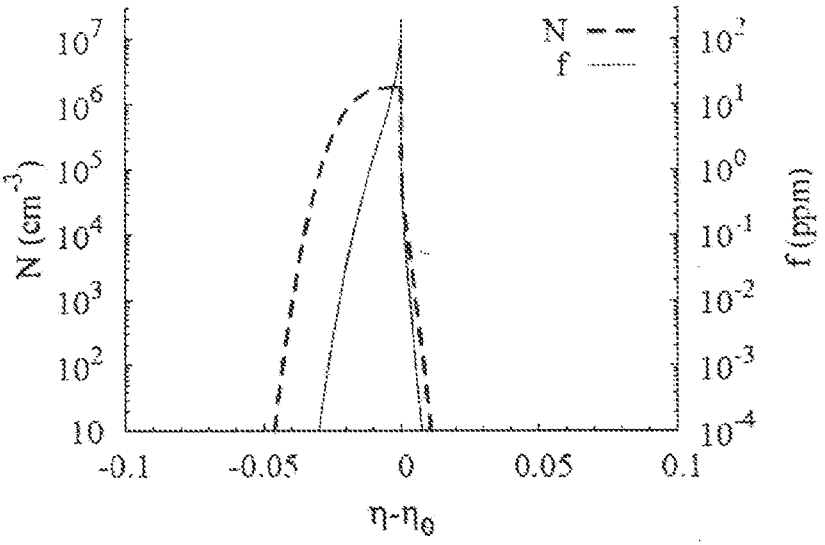
N
f
N (cm^{-3})
f (ppm)
10^7
10^6
10^5
10^4
10^3
10^2
10
10^2
10^1
10^0
10^{-1}
10^{-2}
10^{-3}
10^{-4}
-0.1
-0.05
0
0.05
0.1
$\eta-\eta_0$

FIG. 4A

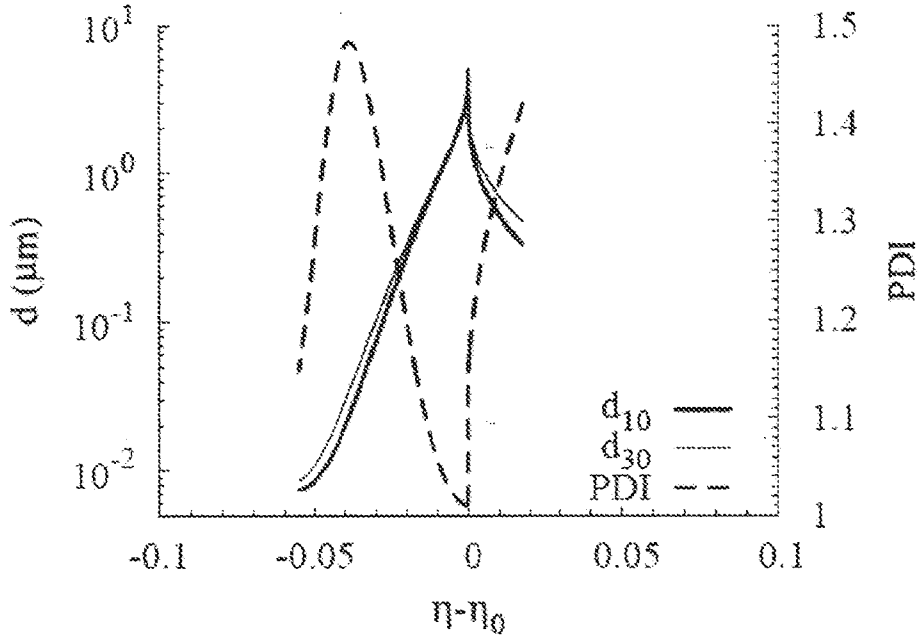
d (µm)
PDI
10^1
10^0
10^{-1}
10^{-2}
1.5
1.4
1.3
1.2
1.1
1
d_{10}
d_{30}
PDI
-0.1
-0.05
0
0.05
0.1
$\eta-\eta_0$

FIG. 4B

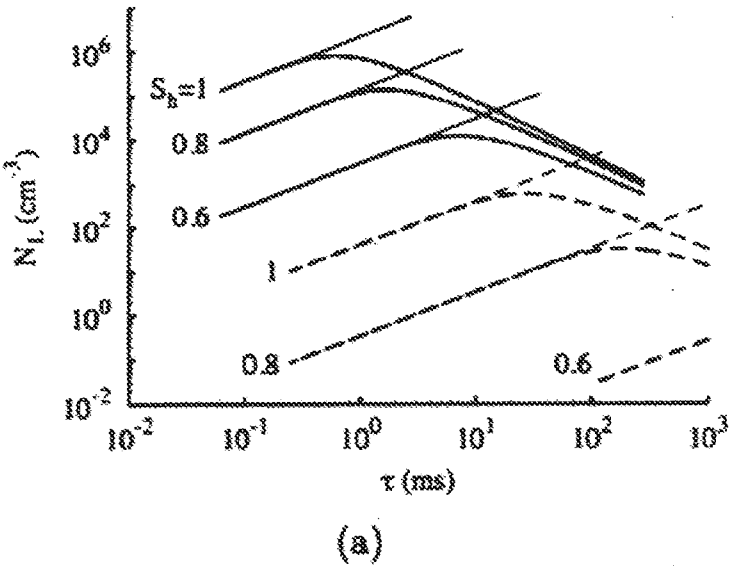

(a)

FIG. 5A

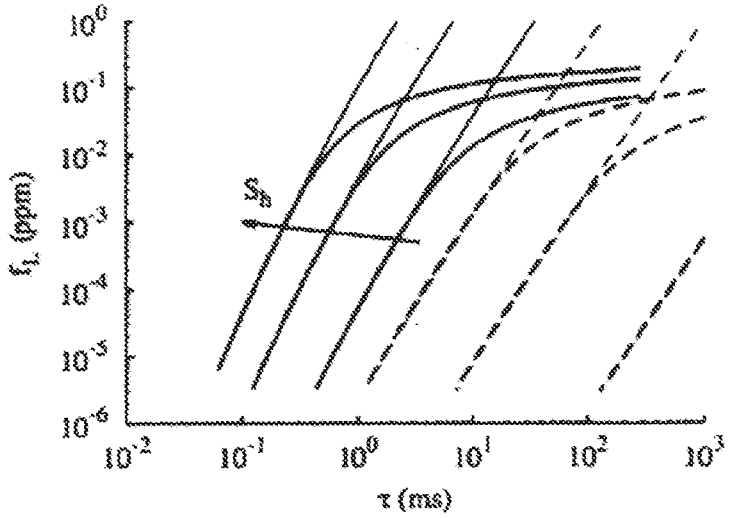

FIG. 5B

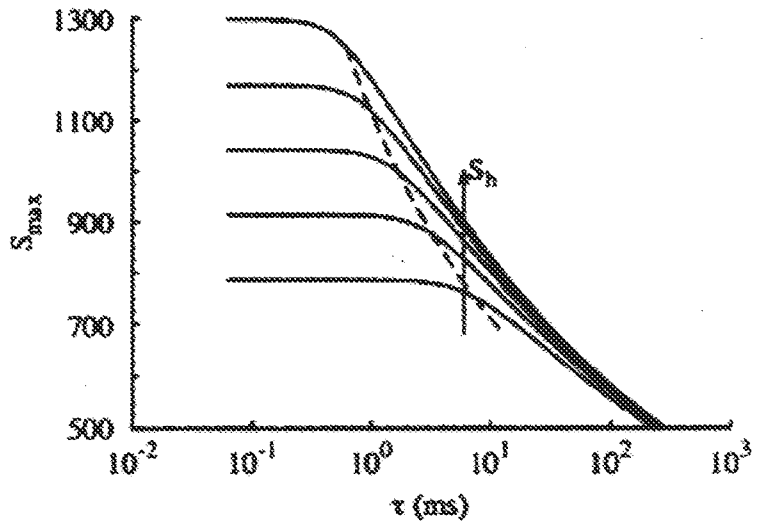
1300
1100
900
700
500
S_{max}
S_h
10^{-2}
10^{-1}
10^{0}
10^{1}
10^{2}
10^{3}
τ (ms)

FIG. 6A

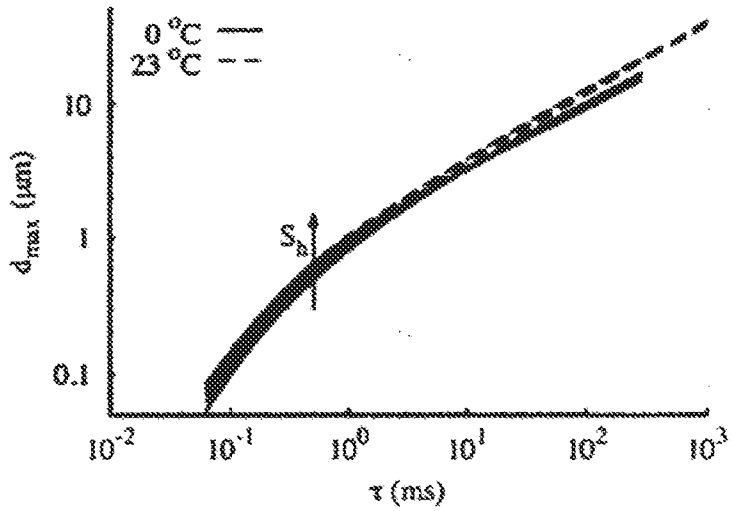
0 °C
23 °C
10
1
0.1
d_{max} (μm)
S_h
10^{-2}
10^{-1}
10^{0}
10^{1}
10^{2}
10^{3}
τ (ms)

FIG. 6B

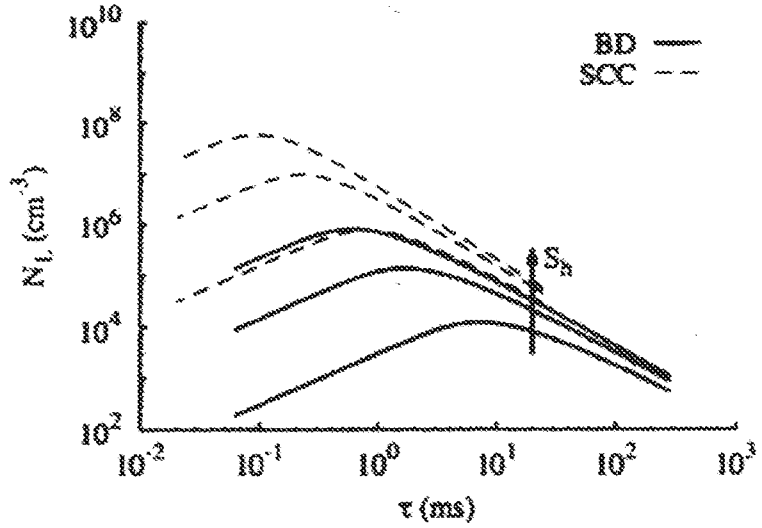
BD
SCC
S_h
N_t (cm^{-3})
10^{10}
10^{8}
10^{6}
10^{4}
10^{2}
10^{-2}
10^{-1}
10^{0}
10^{1}
10^{2}
10^{3}
τ (ms)

FIG. 7A

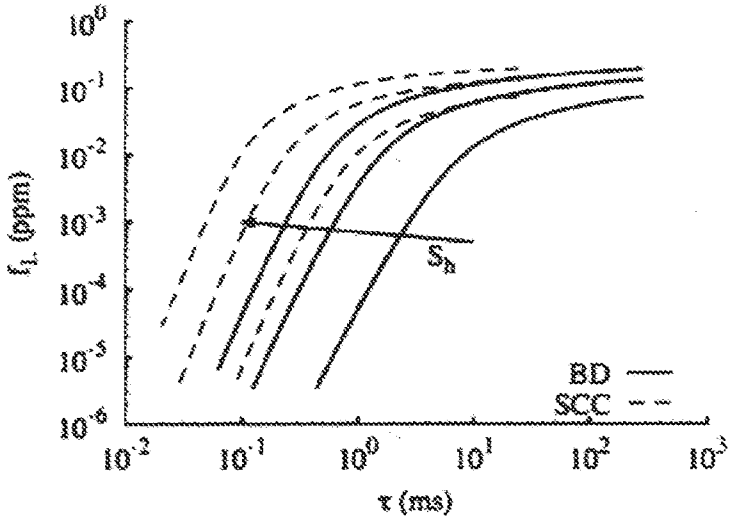
f_t (ppm)
10^{0}
10^{-1}
10^{-2}
10^{-3}
10^{-4}
10^{-5}
10^{-6}
S_h
BD
SCC
10^{-2}
10^{-1}
10^{0}
10^{1}
10^{2}
10^{3}
τ (ms)

FIG. 7B

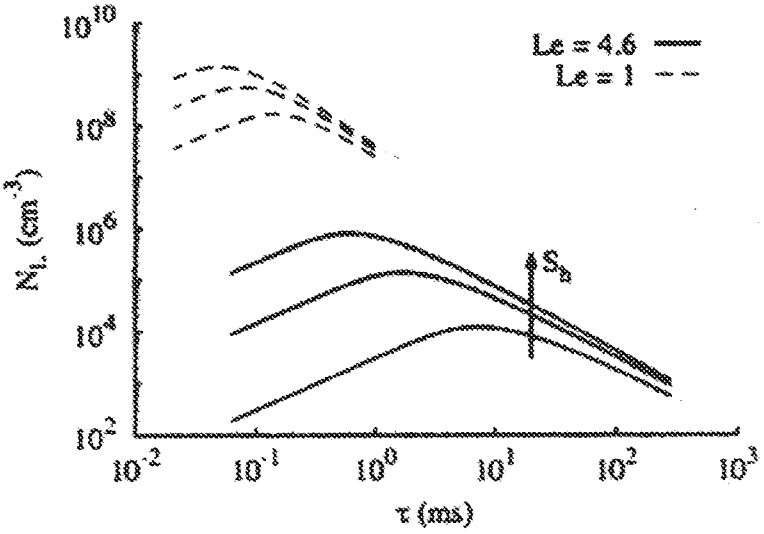
Le = 4.6
Le = 1
S_b
N_t (cm^{-3})
10^{10}
10^{8}
10^{6}
10^{4}
10^{2}
10^{-2}
10^{-1}
10^{0}
10^{1}
10^{2}
10^{3}
τ (ms)

FIG. 8A

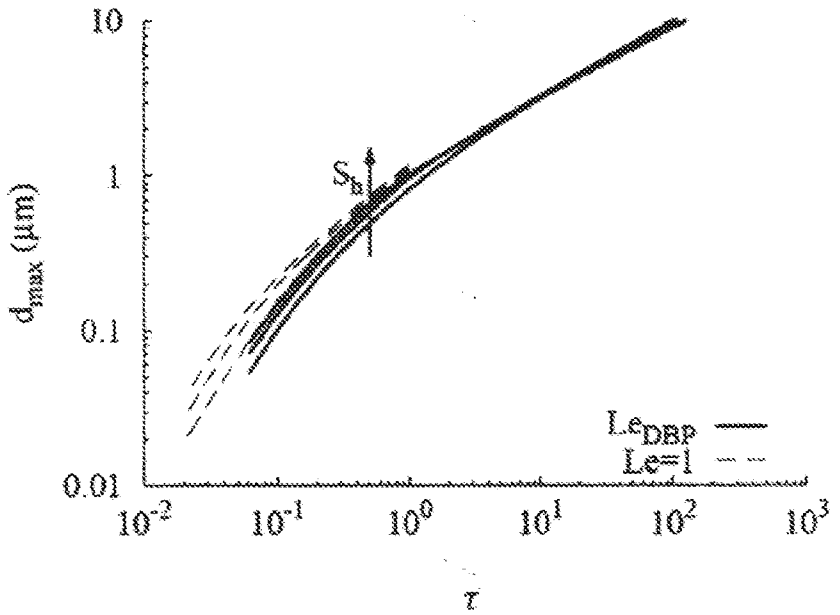
10
1
0.1
0.01
S_b
d_{max} (μm)
Le_{DBP}
Le=1
10^{-2}
10^{-1}
10^{0}
10^{1}
10^{2}
10^{3}
τ

FIG. 8B

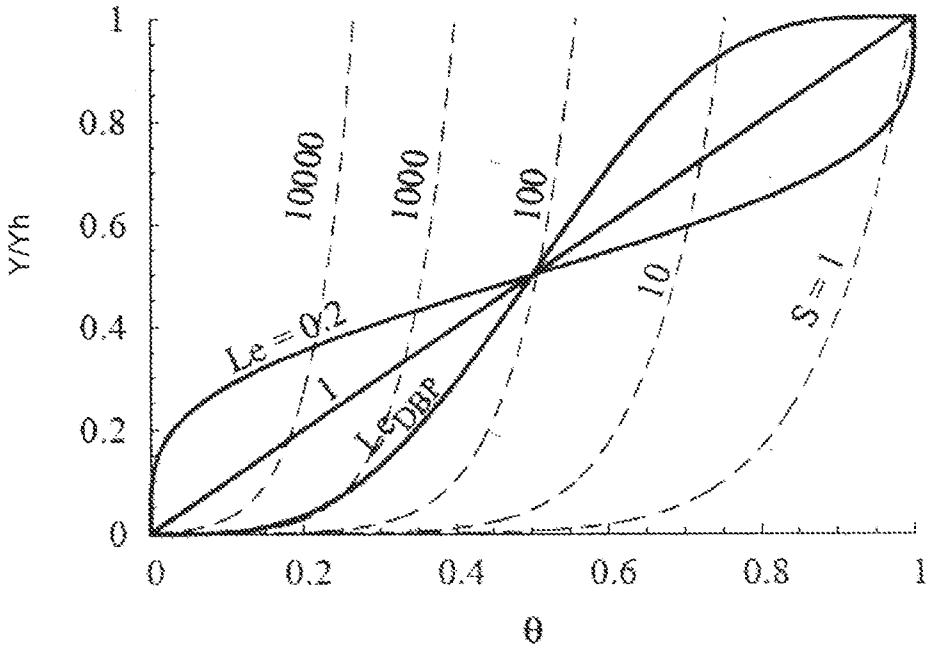
Y/Yh
θ
10000
1000
100
10
S=1
Le = 0.2
1
Le=DSP
0
0.2
0.4
0.6
0.8
1

FIG. 9A

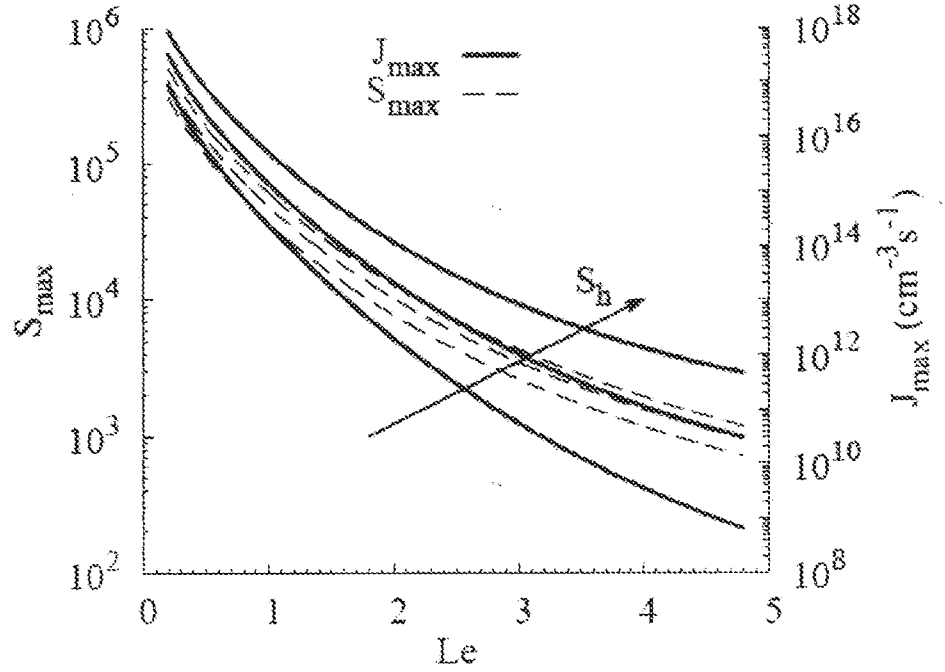
J_{max}
S_{max}
S_h
S_{max}
J_{max} (cm^{-3}s^{-1})
Le
10^6
10^5
10^4
10^3
10^2
10^{18}
10^{16}
10^{14}
10^{12}
10^{10}
10^8
0
1
2
3
4
5

FIG. 9B

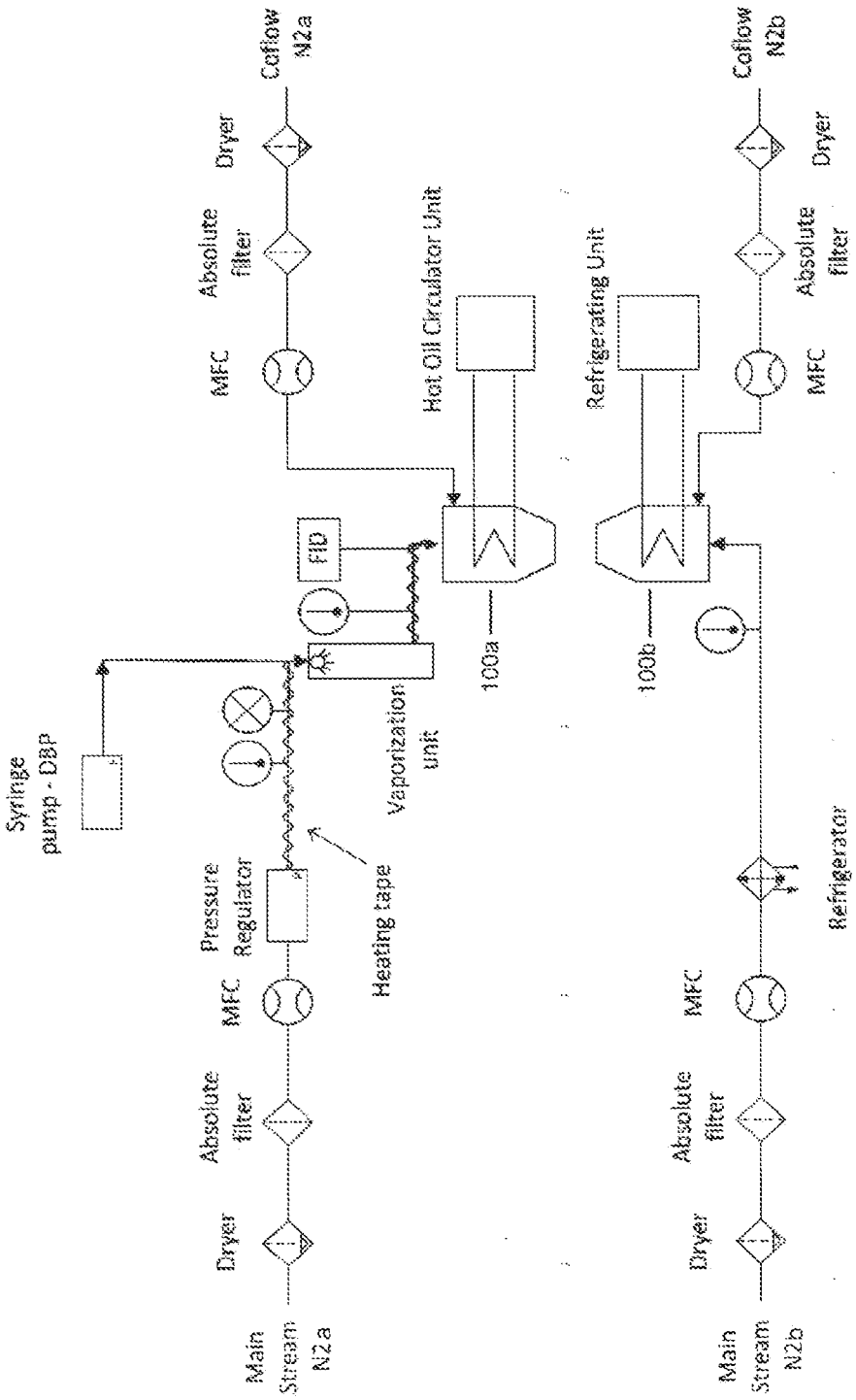
Syringe pump - DBP
Pressure Regulator
MFC
Absolute filter
Dryer
Main Stream N2a
Heating tape
Vaporization unit
FID
100a
Hot Oil Circulator Unit
MFC
Absolute filter
Dryer
Coflow N2a
100b
Refrigerating Unit
MFC
Absolute filter
Dryer
Main Stream N2b
Refrigerator
MFC
Absolute filter
Dryer
Coflow N2b

FIG. 10

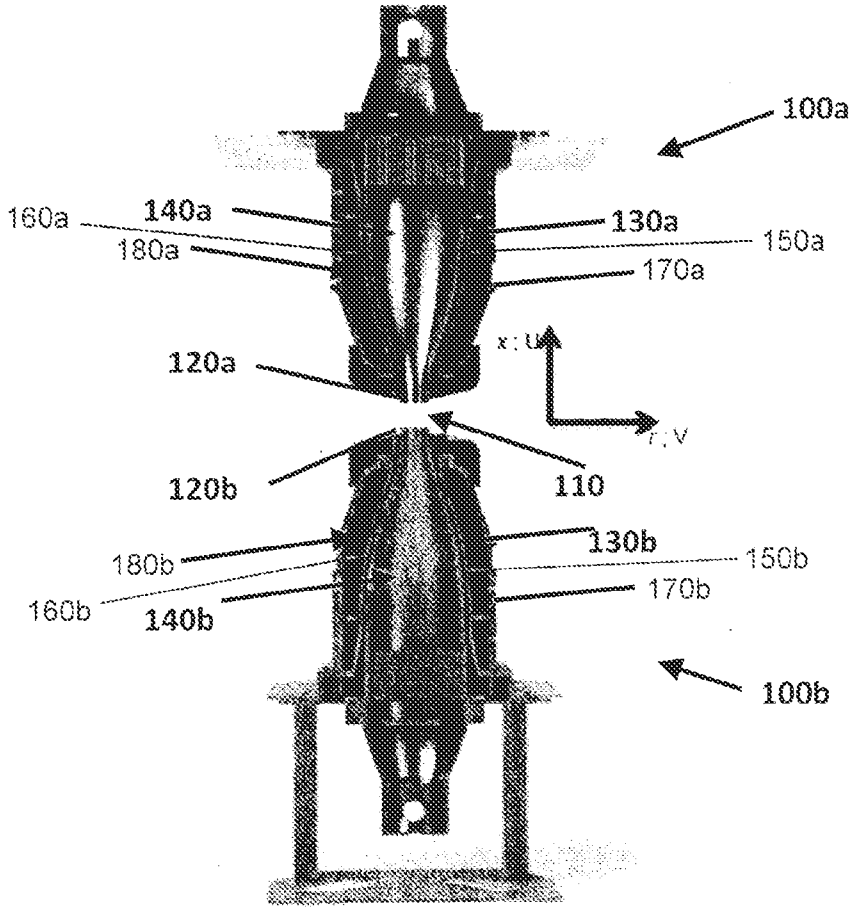
100a
160a
140a
180a
130a
150a
170a
120a
120b
110
180b
130b
150b
160b
140b
170b
100b

FIG. 11A

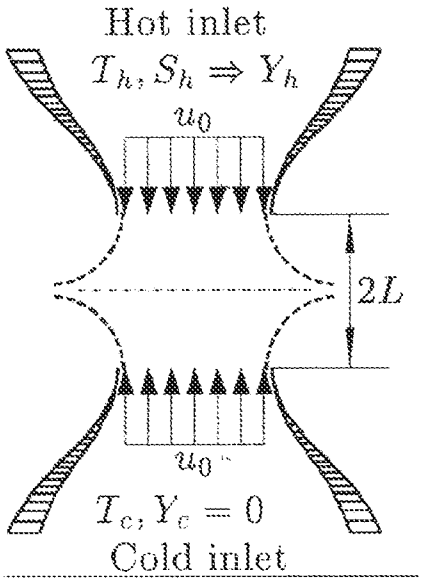

FIG. 11B

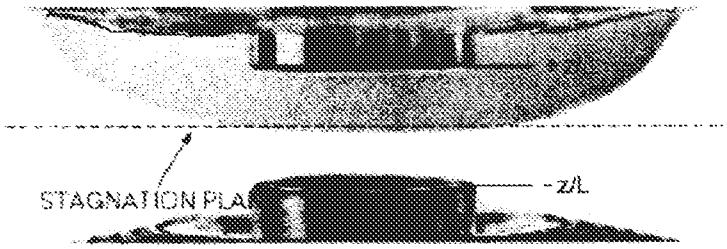

FIG. 11C

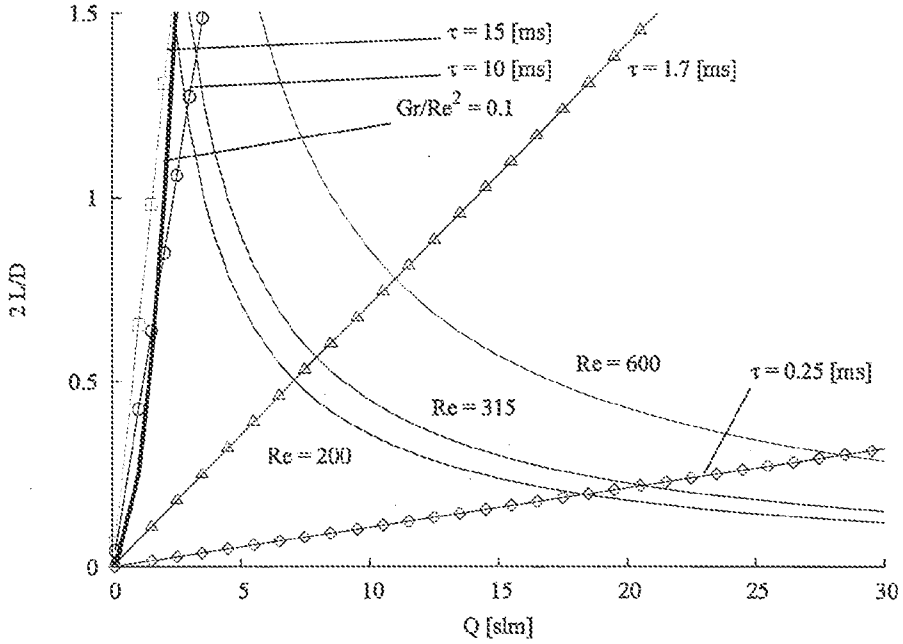
1.5
1
0.5
0
2 L/D
0
5
10
15
20
25
30
Q [slm]
τ = 15 [ms]
τ = 10 [ms]
τ = 1.7 [ms]
Gr/Re^2 = 0.1
Re = 600
τ = 0.25 [ms]
Re = 315
Re = 200

FIG. 12

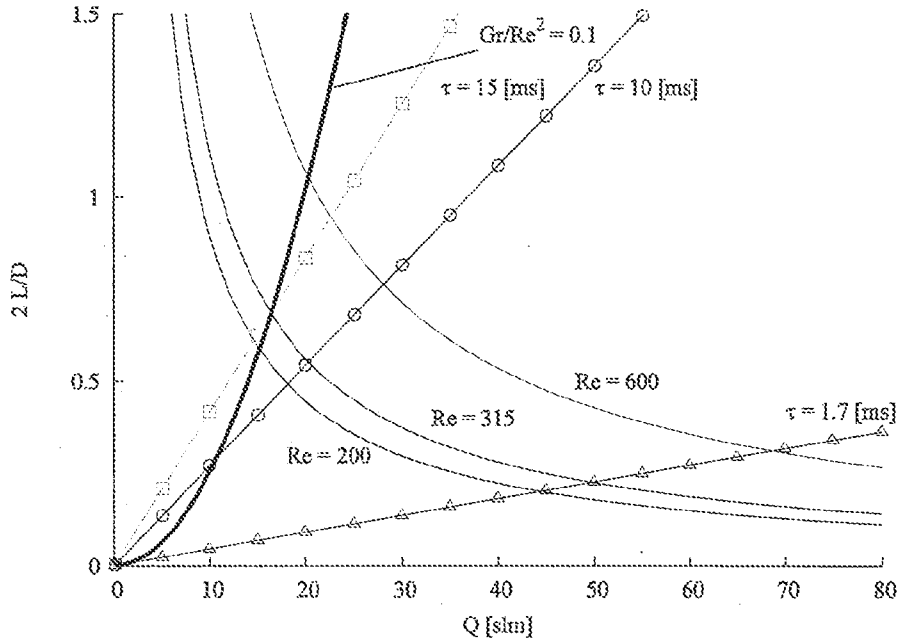
1.5
1
0.5
0
2 L/D
0
10
20
30
40
50
60
70
80
Q [slm]
Gr/Re^2 = 0.1
τ = 15 [ms]
τ = 10 [ms]
Re = 600
Re = 315
τ = 1.7 [ms]
Re = 200

FIG. 13

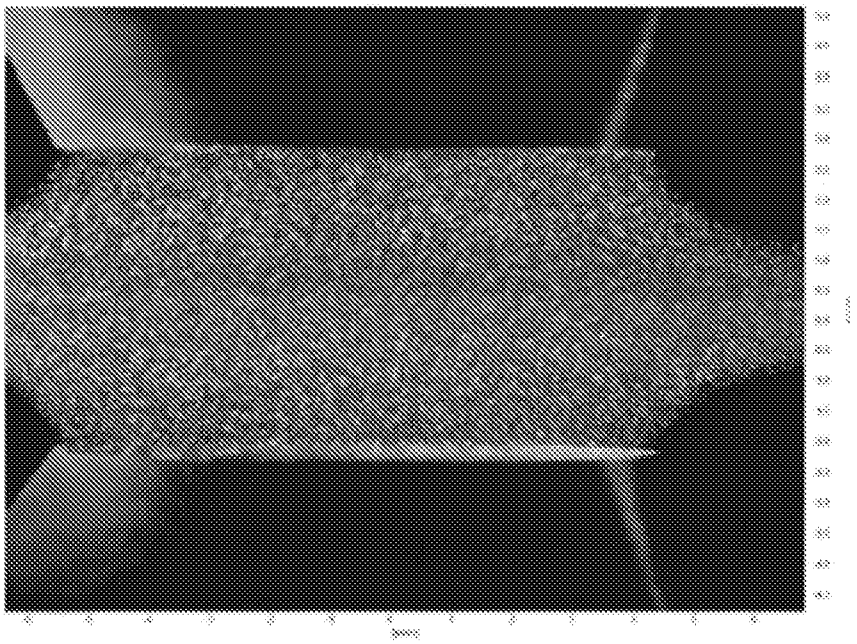

2L / D = 0.5

FIG. 14

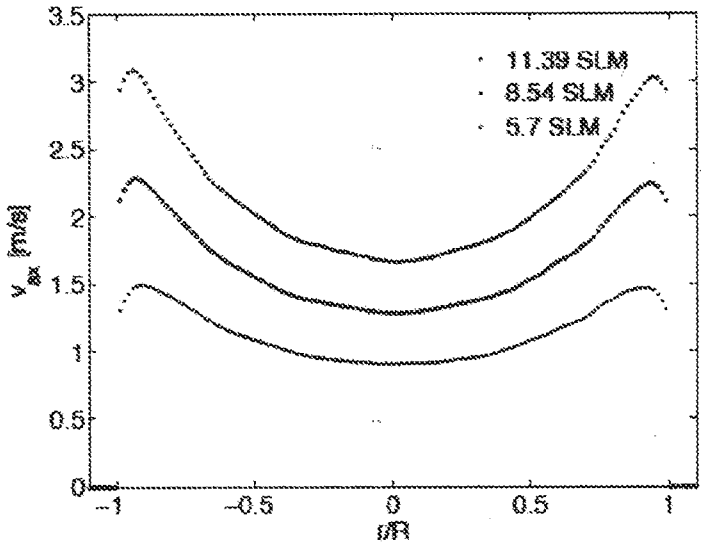
11.39 SLM
8.54 SLM
5.7 SLM
v_{ax} [m/s]
r/R

FIG. 15

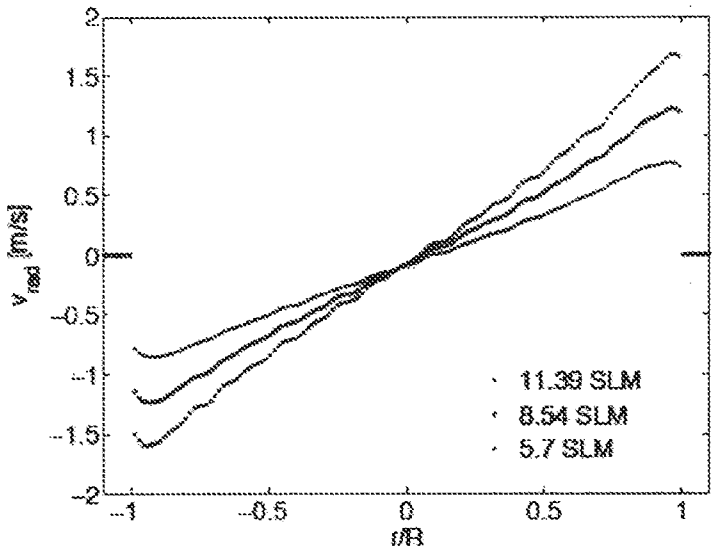
11.39 SLM
8.54 SLM
5.7 SLM
v_{rad} [m/s]
r/R

FIG. 16

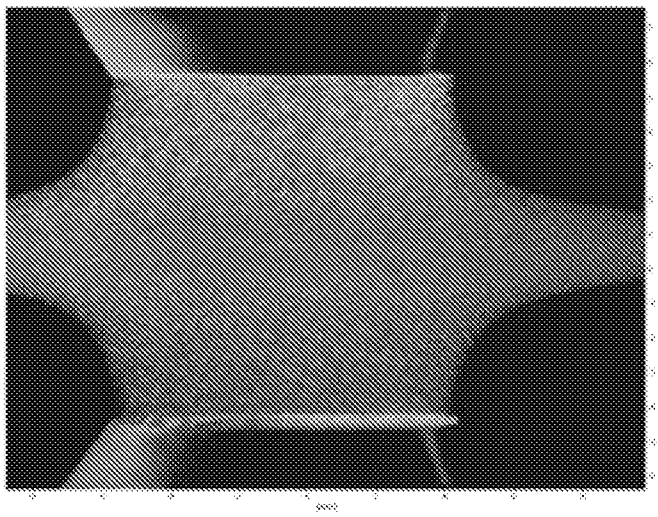

FIG. 17

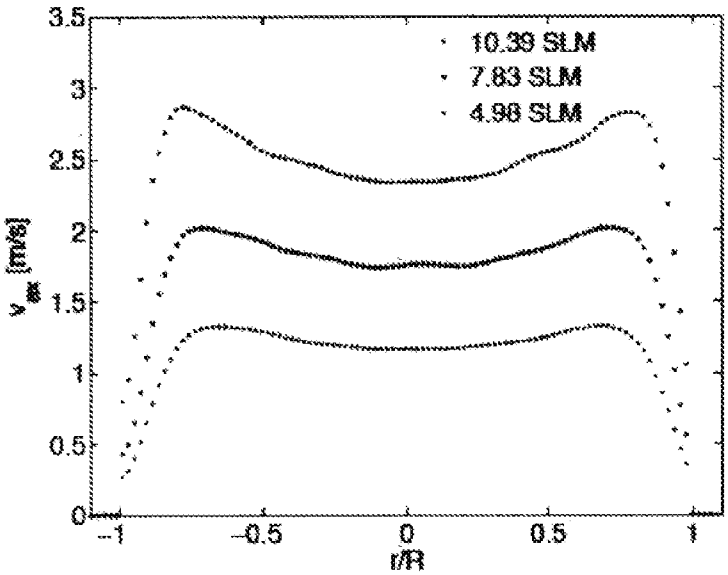

FIG. 18

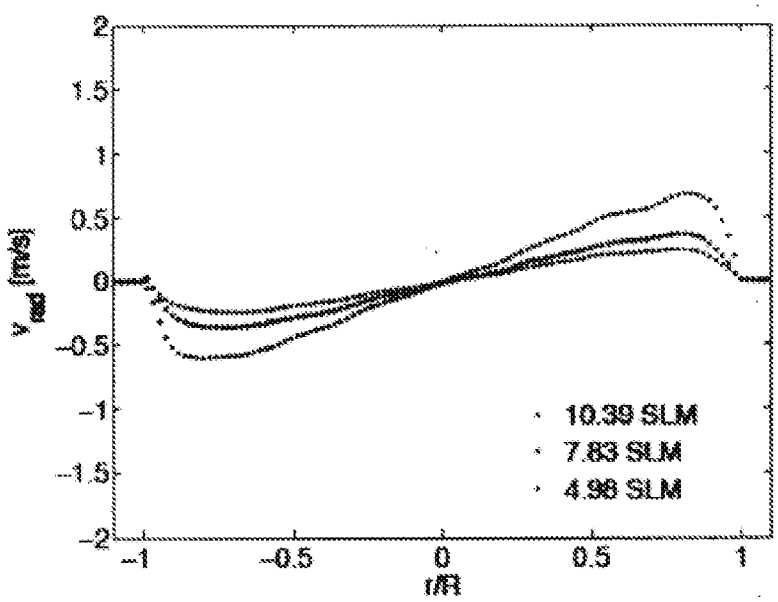

FIG. 19

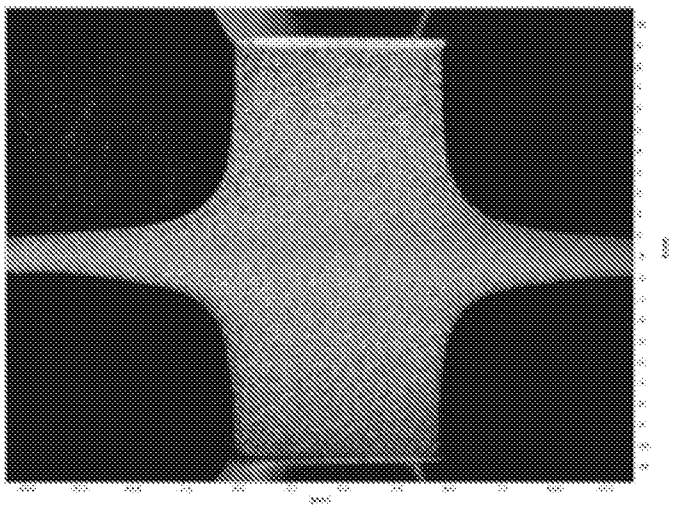

2L / D = 2

FIG. 20

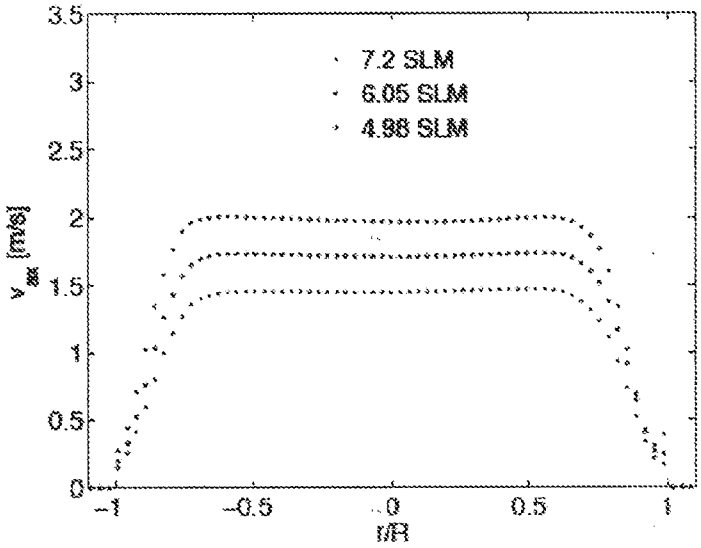

FIG. 21

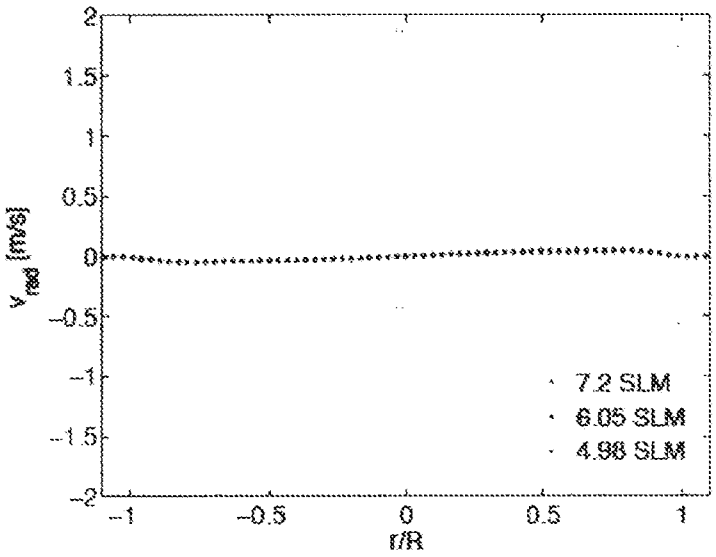

FIG. 22

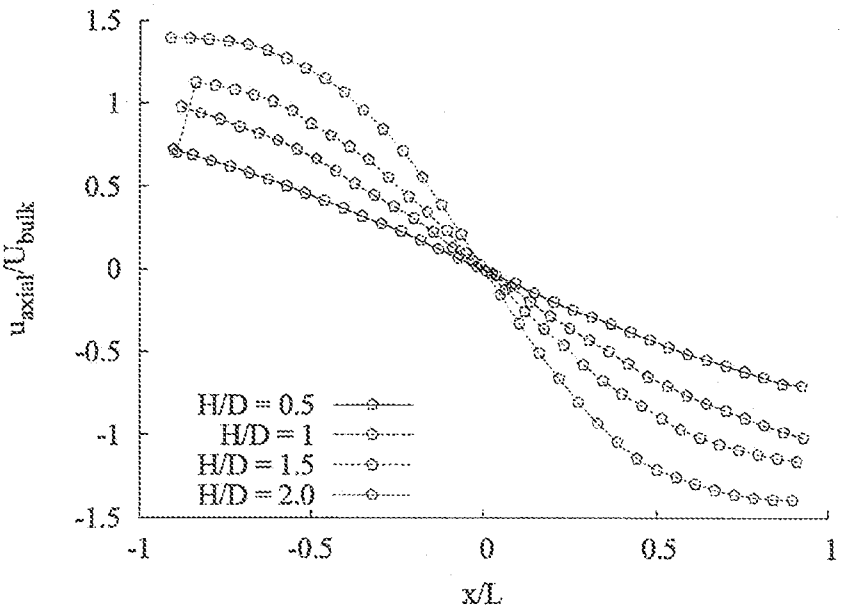
1.5
1
0.5
0
-0.5
-1
-1.5
-1
-0.5
0
0.5
1
u_{axial}/U_{bulk}
x/L
H/D = 0.5
H/D = 1
H/D = 1.5
H/D = 2.0

FIG. 23

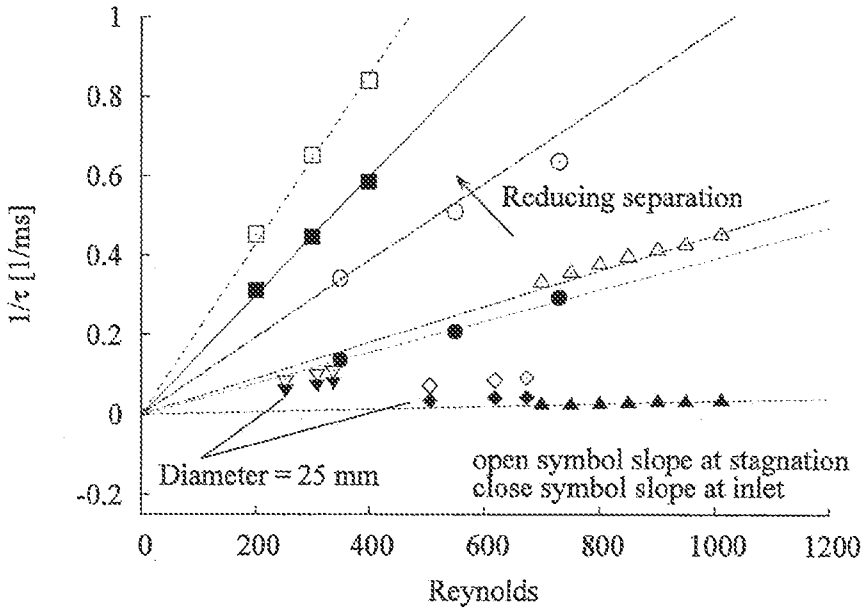
1
0.8
0.6
0.4
0.2
0
-0.2
0
200
400
600
800
1000
1200
1/τ [1/ms]
Reynolds
Reducing separation
Diameter = 25 mm
open symbol slope at stagnation
close symbol slope at inlet

FIG. 24

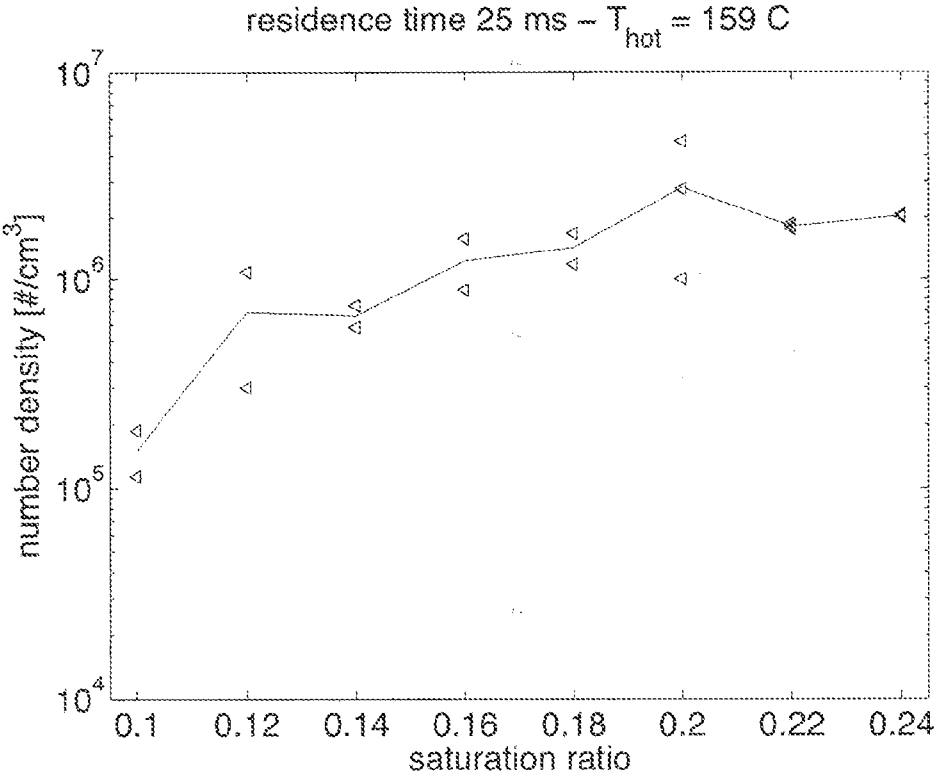
residence time 25 ms – T_{hot} = 159 C
number density [#/cm^3]
10^7
10^6
10^5
10^4
0.1
0.12
0.14
0.16
0.18
0.2
0.22
0.24
saturation ratio

FIG. 25

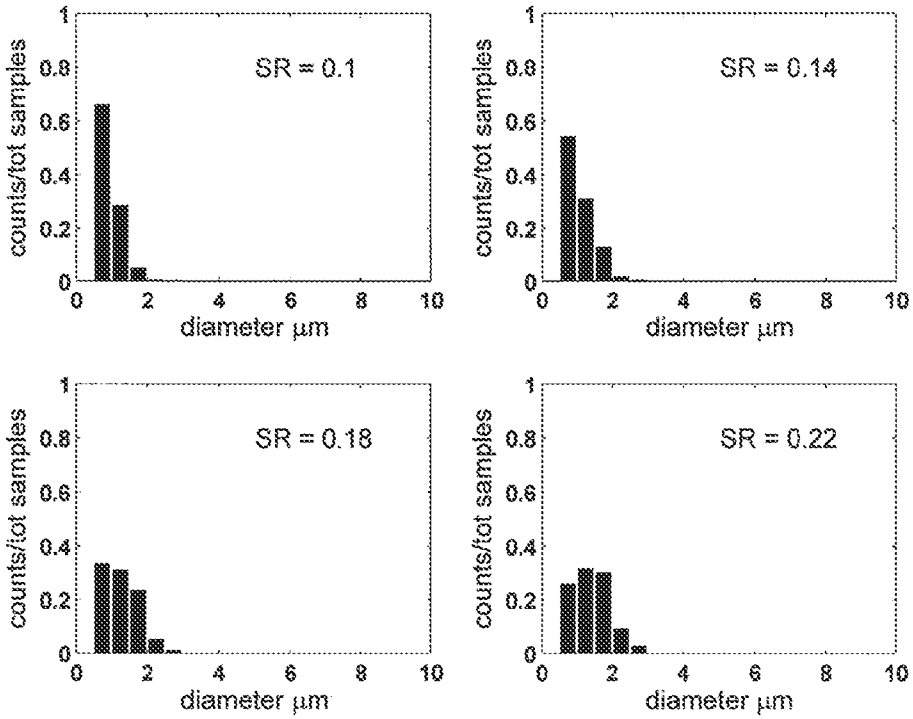
SR = 0.1
SR = 0.14
SR = 0.18
SR = 0.22
counts/tot samples
diameter μm
0
0.2
0.4
0.6
0.8
1
0
2
4
6
8
10

FIG. 26

INTERNATIONAL SEARCH REPORT

International application No
PCT/IB2015/001691

A. CLASSIFICATION OF SUBJECT MATTER
INV. B01J13/00
ADD.

According to International Patent Classification (IPC) or to both national classification and IPC

B. FIELDS SEARCHED

Minimum documentation searched (classification system followed by classification symbols)
B01J

Documentation searched other than minimum documentation to the extent that such documents are included in the fields searched

Electronic data base consulted during the international search (name of data base and, where practicable, search terms used)
EPO-Internal, WPI Data

C. DOCUMENTS CONSIDERED TO BE RELEVANT

Category*	Citation of document, with indication, where appropriate, of the relevant passages	Relevant to claim No.
X	Kun Zhou ET AL: "The effect of residence time on the dynamics of a condensating aerosol in a Hiemenz-type stagnation flow - Abstract Submitted for the DFD13 Meeting of The American Physical Society", , 26 November 2013 (2013-11-26), XP055234909, Retrieved from the Internet: URL:http://absimage.aps.org/image/DFD13/MWS_DFD13-2013-001714.pdf [retrieved on 2015-12-09] the whole document -----	1-14
A	US 2008/083274 A1 (HERING SUSANNE V [US] ET AL) 10 April 2008 (2008-04-10) the whole document -----	1-14

-/--

[X] Further documents are listed in the continuation of Box C.

[X] See patent family annex.

* Special categories of cited documents :

"A" document defining the general state of the art which is not considered to be of particular relevance

"E" earlier application or patent but published on or after the international filing date

"L" document which may throw doubts on priority claim(s) or which is cited to establish the publication date of another citation or other special reason (as specified)

"O" document referring to an oral disclosure, use, exhibition or other means

"P" document published prior to the international filing date but later than the priority date claimed

"T" later document published after the international filing date or priority date and not in conflict with the application but cited to understand the principle or theory underlying the invention

"X" document of particular relevance; the claimed invention cannot be considered novel or cannot be considered to involve an inventive step when the document is taken alone

"Y" document of particular relevance; the claimed invention cannot be considered to involve an inventive step when the document is combined with one or more other such documents, such combination being obvious to a person skilled in the art

"&" document member of the same patent family

Date of the actual completion of the international search	Date of mailing of the international search report
9 December 2015	18/12/2015

Name and mailing address of the ISA/	Authorized officer
European Patent Office, P.B. 5818 Patentlaan 2 NL - 2280 HV Rijswijk Tel. (+31-70) 340-2040, Fax: (+31-70) 340-3016	Tarallo, Anthony

INTERNATIONAL SEARCH REPORT

International application No
PCT/IB2015/001691

C(Continuation). DOCUMENTS CONSIDERED TO BE RELEVANT

Category*	Citation of document, with indication, where appropriate, of the relevant passages	Relevant to claim No.
A	WO 01/27589 A1 (CALIFORNIA INST OF TECHN [US]) 19 April 2001 (2001-04-19) the whole document	1-14
A	WO 99/42200 A1 (SUPERIOR MICROPOWDERS LLC [US]) 26 August 1999 (1999-08-26) the whole document	1-14
A	US 2014/191057 A1 (EAMES CURTIS LEE [US] ET AL) 10 July 2014 (2014-07-10) the whole document	1-14

INTERNATIONAL SEARCH REPORT

Information on patent family members

International application No
PCT/IB2015/001691

Patent document cited in search report	Publication date	Patent family member(s)	Publication date
US 2008083274 A1	10-04-2008	US 2008083274 A1	10-04-2008
		WO 2008045841 A2	17-04-2008
WO 0127589 A1	19-04-2001	EP 1226418 A1	31-07-2002
		US 6567157 B1	20-05-2003
		WO 0127589 A1	19-04-2001
WO 9942200 A1	26-08-1999	AU 2973499 A	06-09-1999
		US 6338809 B1	15-01-2002
		US 6635348 B1	21-10-2003
		US 2005079349 A1	14-04-2005
		US 2005100666 A1	12-05-2005
		US 2005116369 A1	02-06-2005
		US 2007204724 A1	06-09-2007
		US 2007256517 A1	08-11-2007
		US 2007257388 A1	08-11-2007
		US 2010230841 A1	16-09-2010
		US 2011162873 A1	07-07-2011
		WO 9942200 A1	26-08-1999
US 2014191057 A1	10-07-2014	AU 2014203909 A1	06-08-2015
		CA 2896968 A1	10-07-2014
		EP 2941319 A2	11-11-2015
		US 2014191057 A1	10-07-2014
		WO 2014107676 A2	10-07-2014